

CAIPEEX Data workshop

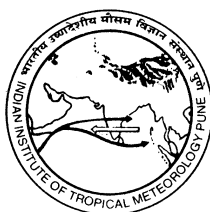
The collage features several key elements:

- A blue and yellow fighter jet in flight.
- A white missile with a red tip.
- A yellow radar dome mounted on a lattice tower.
- A white aircraft labeled "ZS-JRV" with arrows indicating sensor locations.
- Two stacks of electronic equipment.
- A close-up of a yellow sensor assembly.
- Two views of a white aircraft labeled "PCASP" and "AIMMS".
- Labels at the bottom: (c) and (d).
- A weather map overlay in the bottom right corner showing various data points and a legend.

Indian Institute of Tropical Meteorology
Pune - 411 008, India

Report on CAIPEEX Data Workshop (October 2012)

July 2013



Indian Institute of Tropical Meteorology

Dr. Homi Bhabha Road, Pashan Pune - 411 008

Maharashtra, India

E-mail : lip@tropmet.res.in

Fax : 91-020-25865142

Web : <http://www.tropmet.res.in>

Telephone : 91-020-25904200

Preface

Cloud Aerosol Interaction and Precipitation Enhancement EXperiment (CAIPEEX) data workshop was a part of the scientific consultant contracts with National Center for Atmospheric Research (NCAR) and WITS. Experts from NCAR and WITS participated in the workshop to deliver lectures and to train Indian Institute of Tropical Meteorology (IITM) scientists in the data correction and handling procedures for C-band and S-band radar India Meteorological Department IMD () data, various aircraft data inclusive of the radiation and trace gas data collected during the second phase of CAIPEEX 2010. This workshop was organized during for training in the radar data handling and analysis through Thunderstorm Identification, Tracking, Analyses and Nowcasting (TITAN), to investigate how randomized seeding cases can be investigated through TITAN. Several hands on sessions were held as a part of the workshop. The outcome of the hands on and several discussions has been summarized in this short report, which may serve those who are using the data. This report is formulated to increase the knowledge on various datasets from CAIPEEX discussed during the workshop. The report constitutes only the topics discussed during the workshop. Following topics were discussed during the workshop and summaries are prepared on following topics

- Radar Calibration, correction, methods, analysis etc.
- Randomization and statistical methods
- Radar data analysis with TITAN
- Radiation data
- Trace gas data with correction and analysis

Participants of the workshop

Visiting Scientists

Dr. Roelof Bruintjes, RAL/NCAR, USA

Dr. J. Vivekanandan, NCAR, USA

Dr. Stuart Piketh, North-West University
School of Geo and Spatial Science,
Unit for Environmental Science and Management, SA

Dr. Roelof Burger, North-West University
School of Geo and Spatial Science
Unit for Environmental Science and Management, SA

Scientists from IITM

Dr. J.R. Kulkarni
Dr. P.E. Raj
Dr. G. Pandithurai
Dr. R.S. Maheskumar
Dr. (Smt.) S.B. Morwal
Dr. Padmakumari B.
Dr. C.G. Deshpande
Dr. (Smt.) Rohini Bhalwankar
Dr. Mahen Konwar
Dr. Dharmaraj T.
Dr. Sachin Deshpande
Dr. Kaustav Chakravarty
Dr. Subrtakumar Das
Dr. Madhuchandra Reddy
Dr. P. Mukhopadhyaya
Dr. Mahakur
Dr. P. Murugavel
Mrs. Resmi E.A
Ms. Leena
Mr. Subharthi Chaudhuri, CAT
Mr. Sudarshan Bera, CAT
Mr. M.G. Manoj
Dr. (Smt.) Thara Prabhakaran

Students from IITM

Mr. Harikishan G.
Mr. Sachin Patade
Mrs. Gayatri Kulkarni
Miss. Neelam Malap

Acknowledgements

CAIPEEX as Indian national experiment is funded by Ministry of Earth Sciences (MoES).

CAIPEEX team members are thanked for their dedicated contribution in collecting valuable data and making it available to the research community.

Director IITM provided continued support and encouragement for the program, without which this program could not evolve to be successful.

CAIPEEX National Steering Committee provided proper and timely guidance and suggestions in the plan and execution of the experiment.

Several other members of various committees at IITM also contributed to the efforts.

Authors would also like to thank the Library committee and acknowledge the support from LIP.

Dr. D.M. Chate and Dr. A.K. Sahai provided detailed review of this document and their suggestions as reviewers were invaluable.

Theme1

Radar basics, calibration, corrections, Rain Rate estimation



CAIPEEX C-band radar at Mahaboobnagar (Photos from Roelof Burger)

Contributors: S. Morwal, M. Konwar, Roelof Burger, J. Vivekandan, Roelof Bruintjes, T. Prabhakaran

1.1 Basics on Radars

RADAR stands for Radio Detection And Ranging. Radar transmits and receives microwave radiation (pulses). The antenna transmits a narrow beam from the feedhorn suspended on a parabolic antenna. The emitted beam has three fundamental properties (i) pulse repetition frequency (PRF), (ii) transmission time, and (iii) beam width. The PRF is the number of pulses of radiation transmitted per second; transmission time is the duration of each pulse while beam width is the angular width of the emitted beam. The pulse width is also a measure of spacing between two sampling volume and radar range. Figure 1.1 illustrates a simple diagram of radar components.

Once a transmitted beam travels through different atmospheric medium it experiences attenuation due to raindrops, atmospheric gases, small aerosol insects and birds which primarily depends on the operating frequency. Table 1.1 gives denomination of different types of radars and their use. On the range of lowest frequency we can find usual wind profilers, while on the higher frequency side we can find the rain and cloud detection radars.

Table 1.1 Different radars and their characteristics and use

Band	Frequency (GHz)	Wavelength (cm)	Purpose
L	1.3	23	tracking
S	2.8	10.7	rain & hail
C	5.4	5.6	rain & hail
X	9.4	3.2	storm detection
K	24	1.2	cloud detection

The transmitter is a frequency oscillator; most commonly used ones are Magnetron and Klystron. The transmitter produces Radio Frequency (RF) of short duration that transmitted into the atmosphere by the antenna. It can generate the required mean RF power and peak power with a suitable band width. The returned signal i.e. 'echo' is received by a super heterodyne receiver, which transforms the received signal to a lower intermediate frequency (IF). The RF comes from the antenna is applied to a filter, the output being the frequency of the desired frequency band. These frequencies are then applied to the mixer stage which receives input from the local oscillator. A fixed difference in frequency between the local oscillator and the RF signal is maintained by tuning the local oscillator. The IF carrier is applied to the IF amplifier and sent to the detector. The output of the detector is the video component of the input signal.

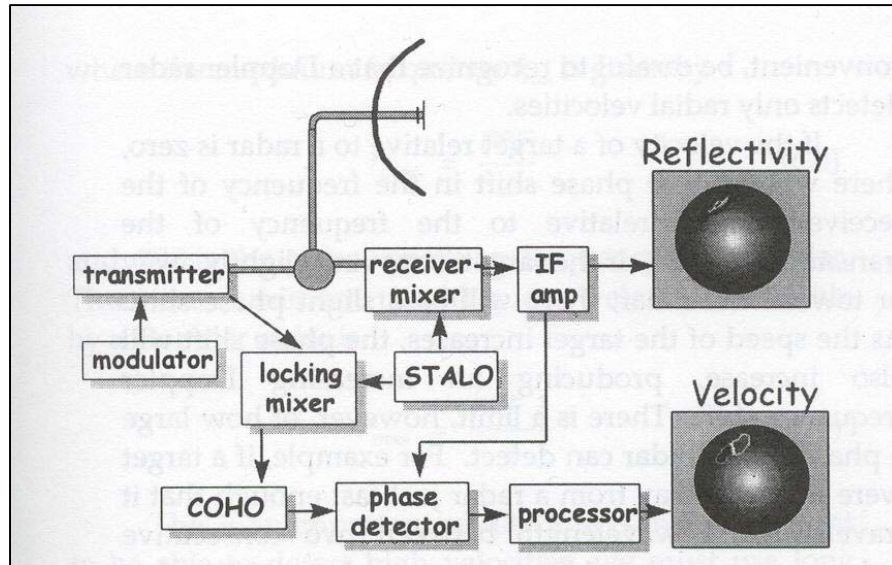


Figure 1.1: Different components of a simple Doppler Radar

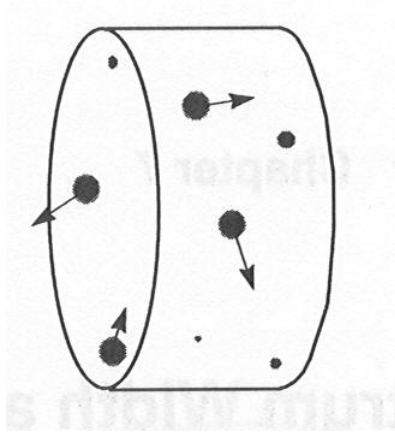
Radar Parameters:

The radar parameters are interpreted from the moments of the received power distribution. The 0th moment i.e. zeroth moment is known as reflectivity, the power returned from a pulse volume. The 1st moment gives the radial velocity while 2nd moment of the power distribution gives spectral width. Radial velocity is a measure of the movement of targets while spectral width gives the turbulence.

The power recorded by the receiver after it reflected back from a target is known as Reflectivity (or echo) which is the most common product of any radar. Its unit is in decibel (dB). Based on the dB range it is possible to determine type of hydrometeors or precipitation e.g. drizzle, heavy rain, graupel or ice. From the radial velocity it is possible to estimate whether a storm is approaching the radar site or moving away. From spectral width one can estimate gust front, updraft or downdraft region or the turbulent region of the storm.

1.2. CAIPEEX 2011 Radar Overview

The Radar Site: Radar was situated in Mahabubnagar which is approximately 85 km from Begumpeth airport, the base of CAIPEEX operations in 2011. The radar was within a distance of 10 km from the IGOC site. The surface elevation of the region and surroundings is given in Figure 1.4a. A hill (< 100m high) very close to the radar was obstructing the radar beam. It was configured to do 10 elevation steps that took about 371 seconds to complete (Figure 4b). The radar was configured to do 400 range bins of 300 meter each out to 120 km. The data were transformed into polar coordinates with a 0.5 degree resolution. The doppler fields were stored, however, the receiver had incorrect calibration factors and the doppler fields were calculated to be within the noise threshold, and therefore eliminated during the transformation from beams to polar coordinates.



- Frequency shift by a moving target: $f = 2 V / \lambda$
(positive velocity – away from the radar; negative velocity – toward the radar)
- Maximum unambiguous frequency shift: $PRF / 2$
- So, maximum unambiguous velocity detectable by a Doppler radar: $V_{max} = PRF \lambda / 4$
(larger velocities cause folding)
- Maximum unambiguous range: $r_{max} = c / (2 PRF)$
(echoes farther away can cause second trip)

c = speed of light ($\sim 3 \times 10^8 \text{ ms}^{-1}$)

PRF = pulse repetition frequency (s^{-1})

Figure 1.2: Radar sample volume containing a few raindrops each with its own speed and direction of movement (left). A real radar volume may have billions of raindrops. Doppler velocity could be estimated from radar as described on the right

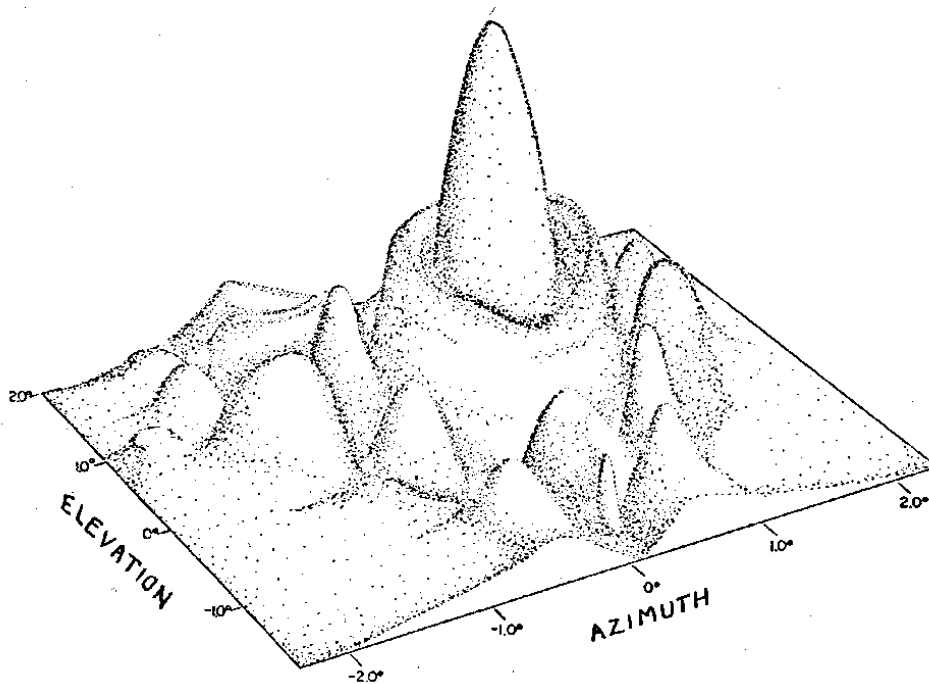


Figure 1.3: Antenna pattern with main and side lobes

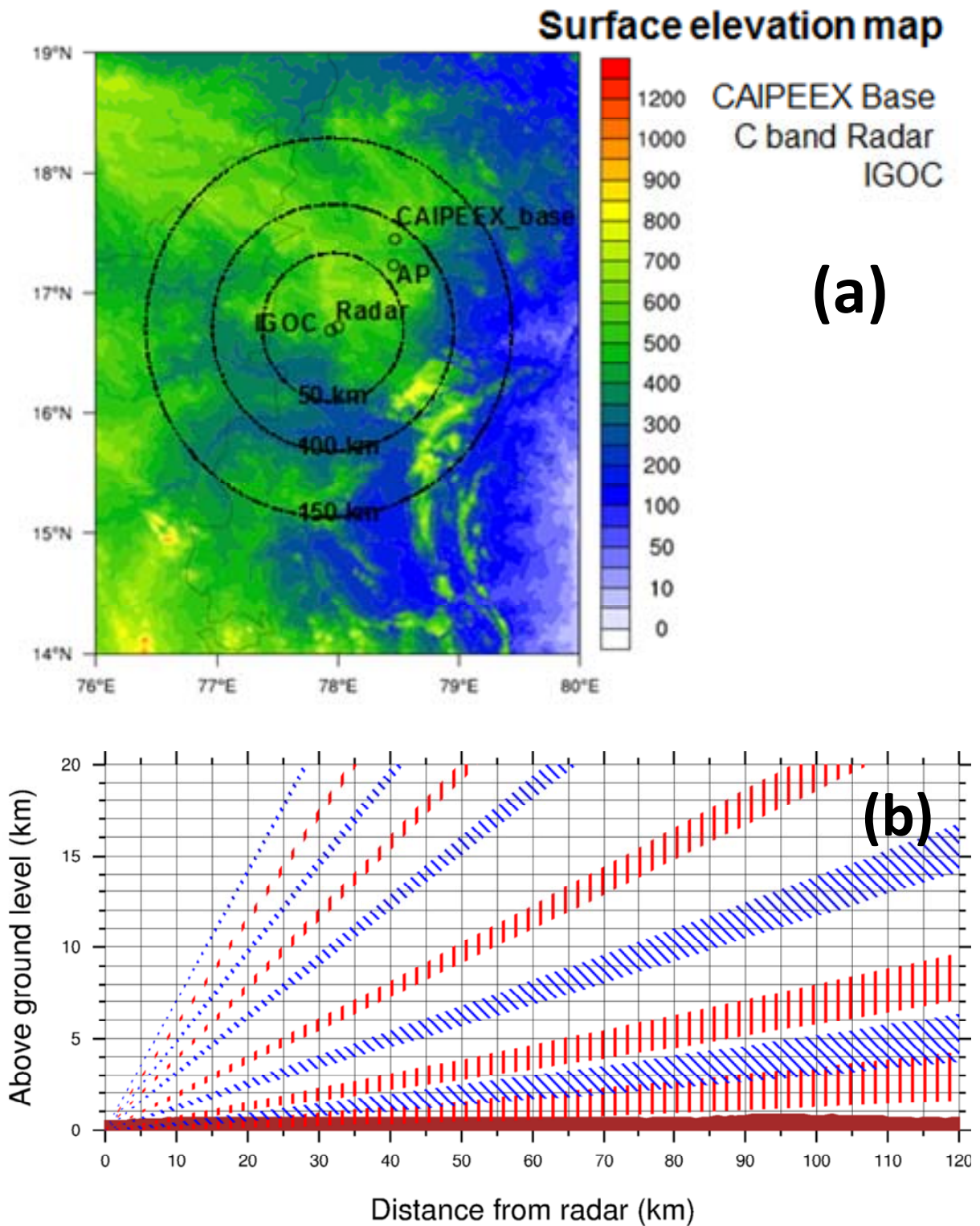


Figure 1.4: (a) Radar location and (b) volume scan strategy of C-Band radar used in the campaign

Specification of the C-band Radar installed at Mahabubnagar, Hyderabad

- Frequency: 5.629 GHz
- Power: 250 kW
- Upgraded by Advanced Radar Corporation ARC in 2010
- Beams angles: 1,2,3.6,7,11,18,23,29,35,45 °

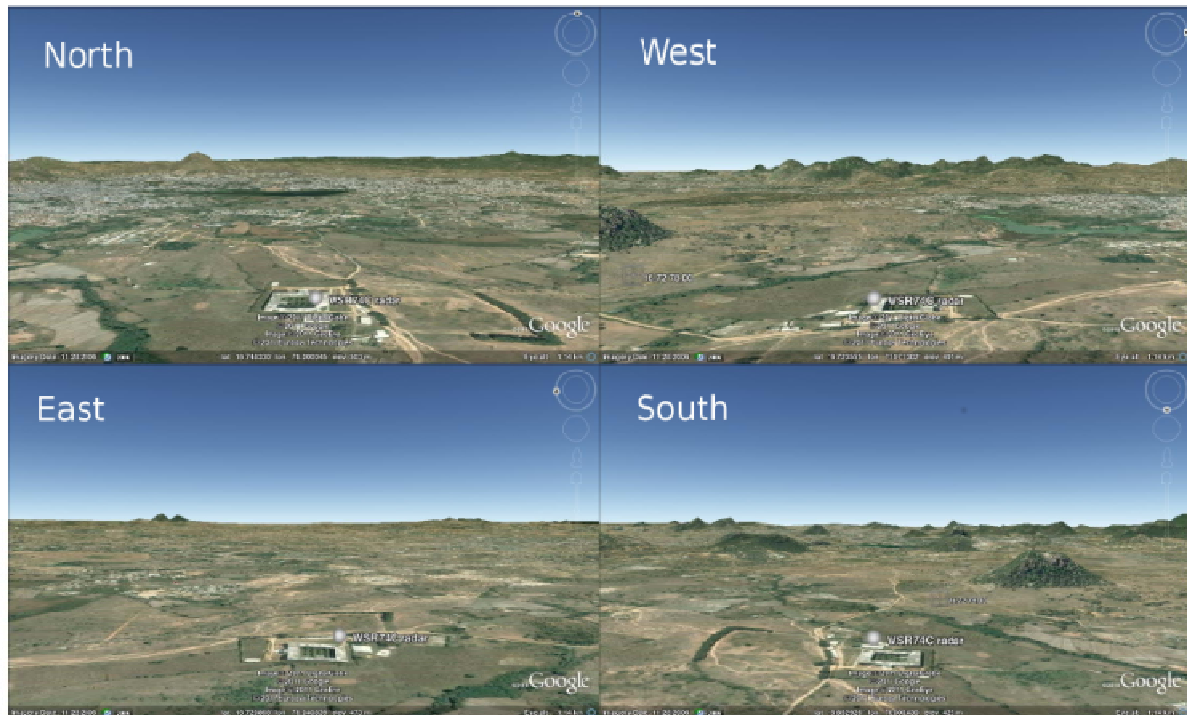


Figure 1.4c: Idealized views from the radar site, showing Google Earth perspectives in different directions using exaggerated topography

Errors in initial calibration

- Waveguide leak
- Transmitter was not set to full power
- RF burst was not uniform, it was 250 ms short
- Incorrect pedestal gear ratio
- Amplifier was not 100% functional

Waveguide leak and the incorrect pedestal gear ratio, caused data quality issues that could not be post-corrected. As a result the following data quality issues remain in the quality controlled data. The original transmitter power was estimated to be down approximately 3 dB. When a calibration was first attempted the HiQ receiver could not be driven into saturation and the sensitivity was very low. Further investigation showed that the IF amplifier in the down converter was not operating. The amplifier was replaced and a good calibration was obtained at 1.0 microseconds

Although low sensitivity, spatial uncertainty, and extreme beam blockage remain with radar data of 2011 and care should be practiced while investigating the individual storm characteristics. The error could vary with the analysis of individual storms and their position, etc. However, this radar data could be invaluable in assessing the statistics of storms

The spatial distribution of storms are presented in Figure 1.5a. This figure also gives the topography in the background. Maximum number of storms can be seen on the slopes of mountain ranges in the NE sector. This spatial distribution is doubted and should be analysed with care.

A simple beam propagation algorithm was used to calculate the lowest usable constant altitude plan position indicator (CAPPI) (Figure 1.5b). The impact of the hill just to the South West is not fully captured, but the degradation of low altitude CAPPIs to the South is clear. Even to the North a lot of irregularities in the lower CAPPIs. This will contaminate data in the lower levels. From 1.5 it is clear that data below 4km should be viewed with great caution in the area of interest. Artifacts is likely even above this level towards the South. These artifacts proved useful in correcting the gear-ratio problem .

Gear ratio: The C-band radar had an incorrect gear-ratio configured. Since absolute encoder motors were used, this resulted in a variable error in the azimuth of the antenna. The distinctive blockage of the topography (Figure 1.4a) was noted and this pattern slowly rotated with each turn of the antenna. During the campaign, maintenance were done on the antenna and this introduced further discreet jumps in the azimuth offset. The largest blockage in the lowest elevation is as a result of the small hill towards the South, The wedge of blockage should therefore be 212.7 degrees from true North.

Radar data is provided in .mdv format due to the space requirements. It is recommended to use an mdv2netCDF in TITAN software to make conversions to netCDF format if required.

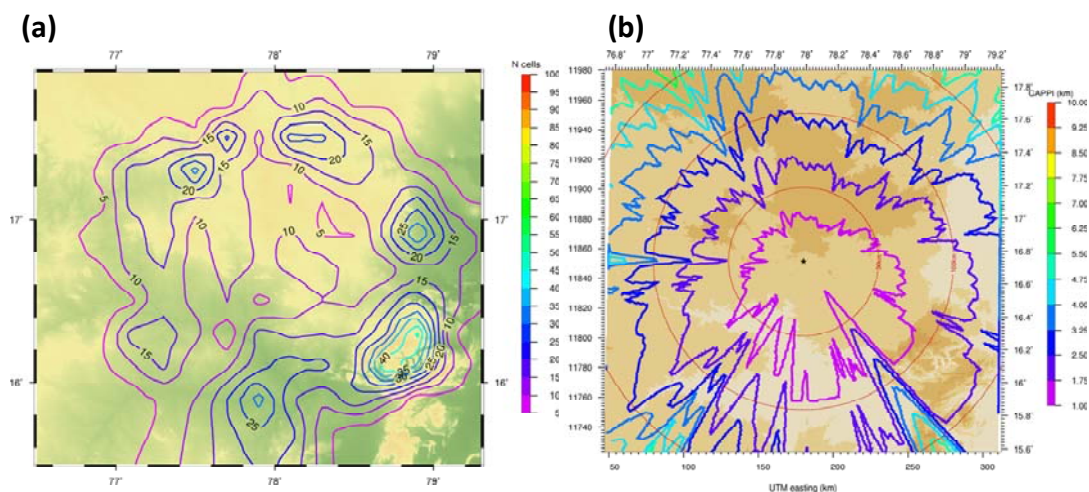


Figure 1.5: Storm distribution around radar (a) and lowest CAPPIs (Constant Altitude Plan Position Indicator) (b) Note that over the southeastern sector there are strong topography effects

The top frame in Figure 1.6 shows the total daily storm areas for the period. From this it can be seen that days with many and/or big storms and days when there were little or no activity. Notice the logarithmic scale on the y-axis. The second frame in figure 1.6 shows the number of storms on each day that reach tops above 6 km. The scale annotates the number of storms for each height on a particular day. It is evident that storms reached maximum tops just over 12km. The third frame in figure 1.6 shows the number of storms on each day that reach a maximum reflectivity as annotated on the scale. It shows that the maximum reflectivity is typically around 55dbz. The bottom frame in figure 1.6 shows the number of storms on each day

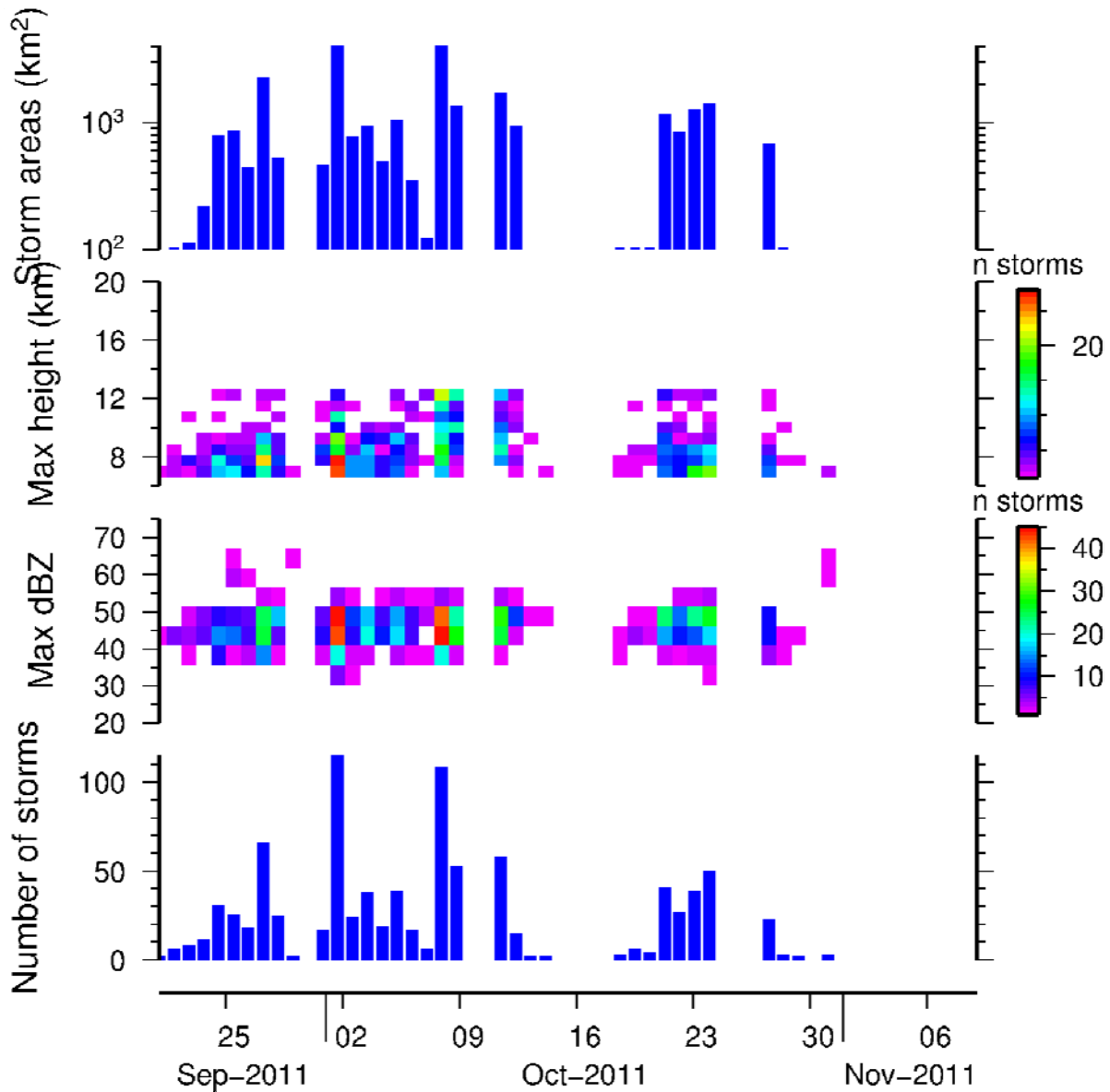


Figure 1.6: A summary of general statistics from CAIPEEX radar

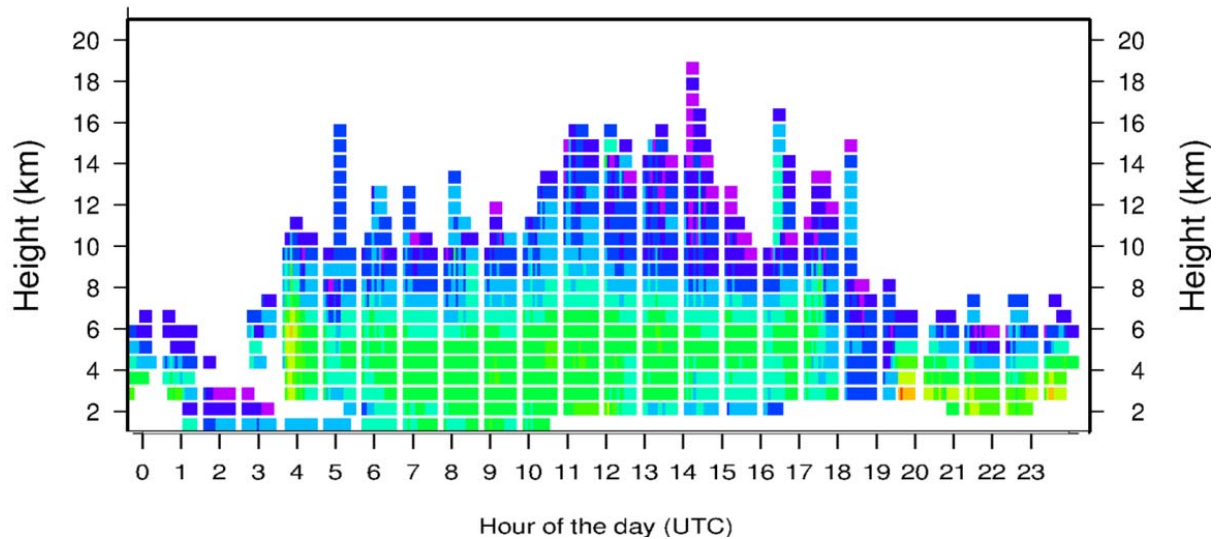


Figure 1.7: Diurnal distribution of cells, indicative of deeper cells during the second half of the day, while low to medium cells dominate throughout the day. No deep cells were reported during the night

1.3 Radar calibration and Rain Rate Estimation

Radar calibration: Background

Power calibration:

- Z (radar reflectivity): 0.5 to 1 dB (for Doppler radar)
- Z_{DR} (Differential reflectivity): 0.1 to 0.2 dB (for polarization Radar)
- L_{DR} (Linear depolarization Ratio): 1 to 2 dB (for polarization Radar)

Errors: Systematic Errors

- Random errors (these can be reduced by averaging)
- More accuracy is required for rain rate estimation than for PID (Particle identification)
- Maintenance of an initial calibration

Single polarization radar versus dual polarization radar calibration

- Rain gauge and radar-based rain rate comparison
- Self-consistent techniques
- Bias in reflectivity (directly affects the rain rate estimation)
- Variability in drop size distributions
- Attenuation of radar measurements
- Direct comparison of radar observation versus tuning of Z-R (rainfall rate) coefficients

Single channel Radar calibration

External calibration

Methods

- Perfectly conducting sphere
- External calibration source
- Solar calibration (this can be done daily)

After this the comparison of Drop size distribution using radar and disdrometers is explained. Also the diurnal variation of drop diameter, reflectivity and rain rate using radar were shown which show one-to-one variation with time.

Calibration procedure

- Using fixed target
- Selection criteria for fixed target are:
 - Fixed structure: tall buildings or mast or tower
 - Ground and vegetation show changes because of soil moisture
 - Short ranges are preferred in order to reduce the variability due to change in refractive index with distance
- Stronger signals return with reflectivity more than 50 dBZ it means that it is stronger than the surrounding ground clutter
- Target location should be well above the radar horizon and at ranges between 2 to 4 km

Then it was explained with the help of an example.

Calibration techniques: influencing Factors

- Raindrop size distribution
- Raindrop shape
- Statistical fluctuation in measurements
- Gaseous absorption
- Attenuation due to precipitation

The above influence was explained in detail with the help of equations and different size distributions.

After, the self-consistency calibration procedure was explained for polarization radars:

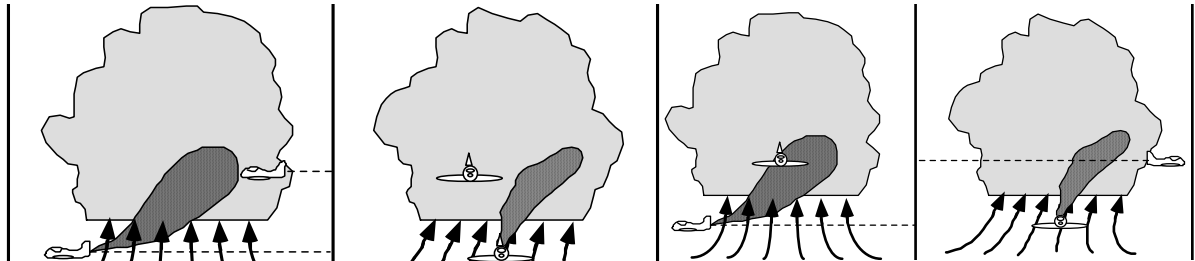
- Select radial radar data in rain that are free from any ice and ground clutter.
- Compute K_{DP} (Specific differential phase) at each range gate using Z and Z_{DR} .
- Sum the K_{DP} along the radial to obtain the estimated ΦDP (Differential propagation phase).
- Compute reflectivity bias as estimated ΦDP /measured ΦDP .
- Process sufficient # of rays to obtain a mean value of the bias.

Summary:

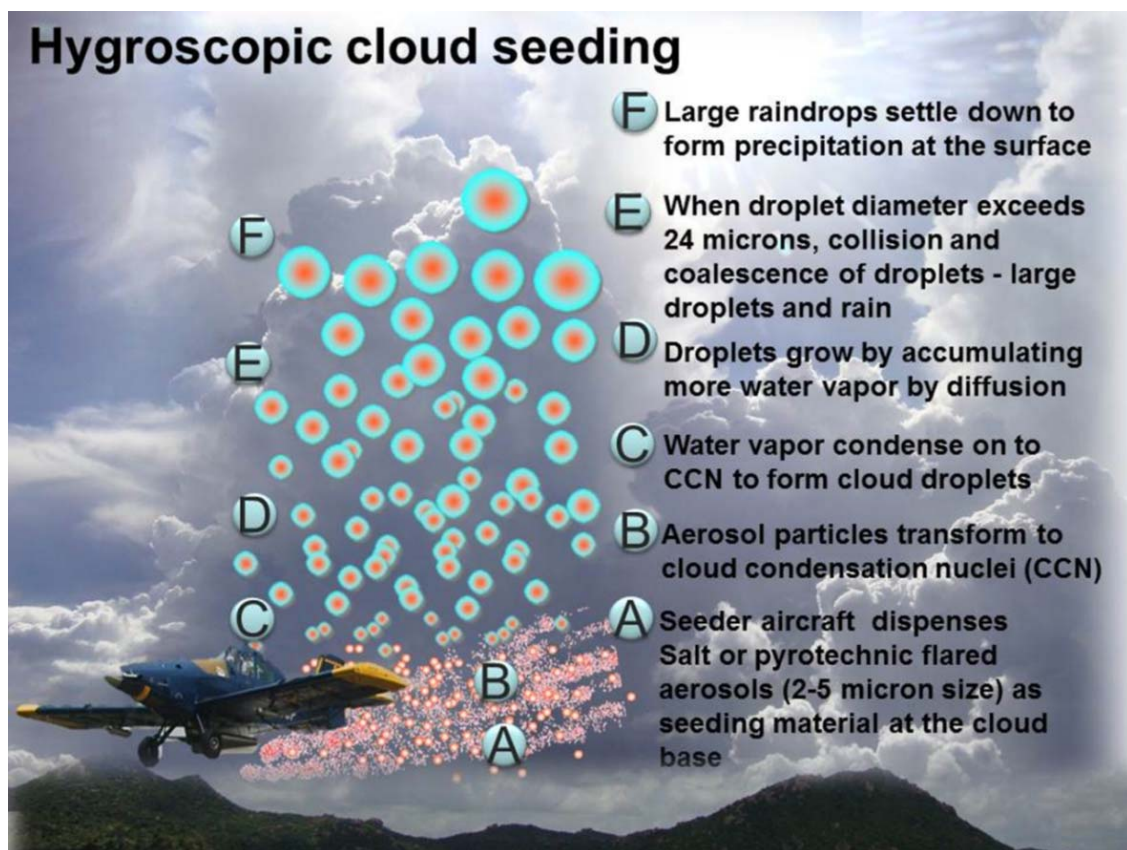
- Internal calibration using built in test in equipment.
- Metal sphere: 'End-to-end' calibration
- Solar calibration: One-way receiver gain calibration.
- Tower and tower mounted targets: Highly repeatable.
- Standard gain horn and test signal: Antenna pattern measurements.
- Co-located and non-collocated disdrometer observations are better than rain gauge measurements
- Self-consistent measurements in rain: Polarization radar

Theme 2

Hygroscopic cloud seeding and Randomization



Hygroscopic material dispensed from an aircraft at the base of the cloud, while another aircraft samples the cloud at 1000 ft above cloud base to capture the seeding material plume that gets spread in to the cloud body



(Photos and sketch by T. Prabha)

Contributors: T. Prabhakaran, J. R. Kulkarni, Roelof Bruintjes

Introduction

Water vapor in the air condenses on hygroscopic particles which act as cloud condensation nuclei (CCN), (a specific kind of water-soluble aerosol) to form cloud droplets. Droplet growth by condensation occurs through diffusion of water vapor. Cloud droplets are typically in the size range of 5-25 microns and characterize very small terminal velocity. This does not lead to any precipitation. The water stays in the cloud to increase the life time of cloud. The collision and coalescence of droplets falling at different terminal velocities can lead to raindrop formation as illustrated in Figure 2.1.

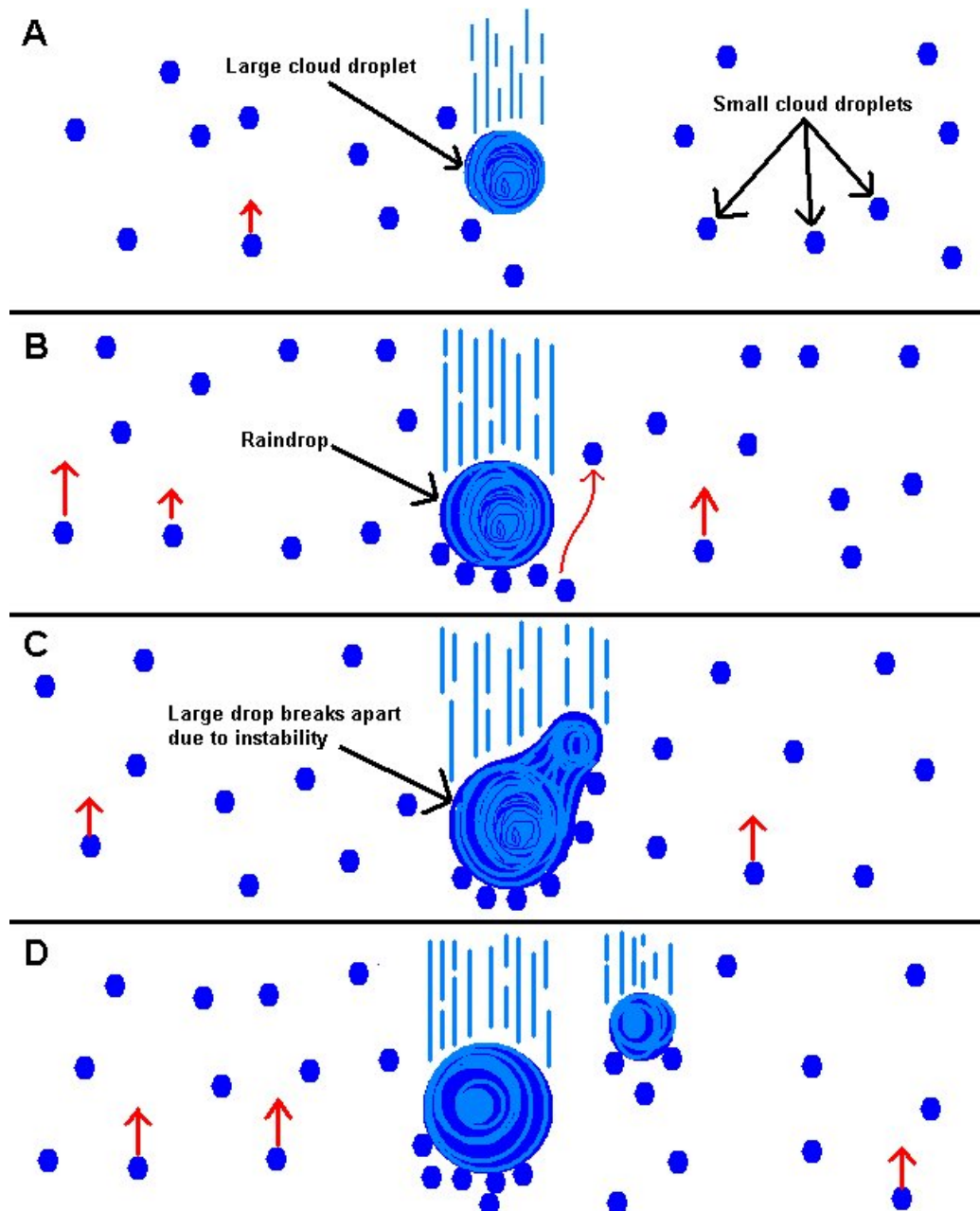


Figure 2.1: Falling of large cloud droplets and collision and coalescence to form large drops and rain drops. (Note that cloud droplets are 100 time smaller in diameter than the rain drops)

Ice nuclei are a subset of aerosol particles and can form ice crystal formation through primary nucleation. There is secondary ice nucleation through various other processes without the aid of ice nuclei and due to this aspect; it is always difficult to relate the ice nuclei concentration with the ice crystals observed in clouds. Co-existence of ice crystals and super cooled droplets leads to rapid vapor growth of crystals, followed in suitable convective clouds by accretion growth (riming), fall-out, and melting as rain. There are various microphysical processes (Figure 2.2) in a cloud which is having both water and ice as illustrated.

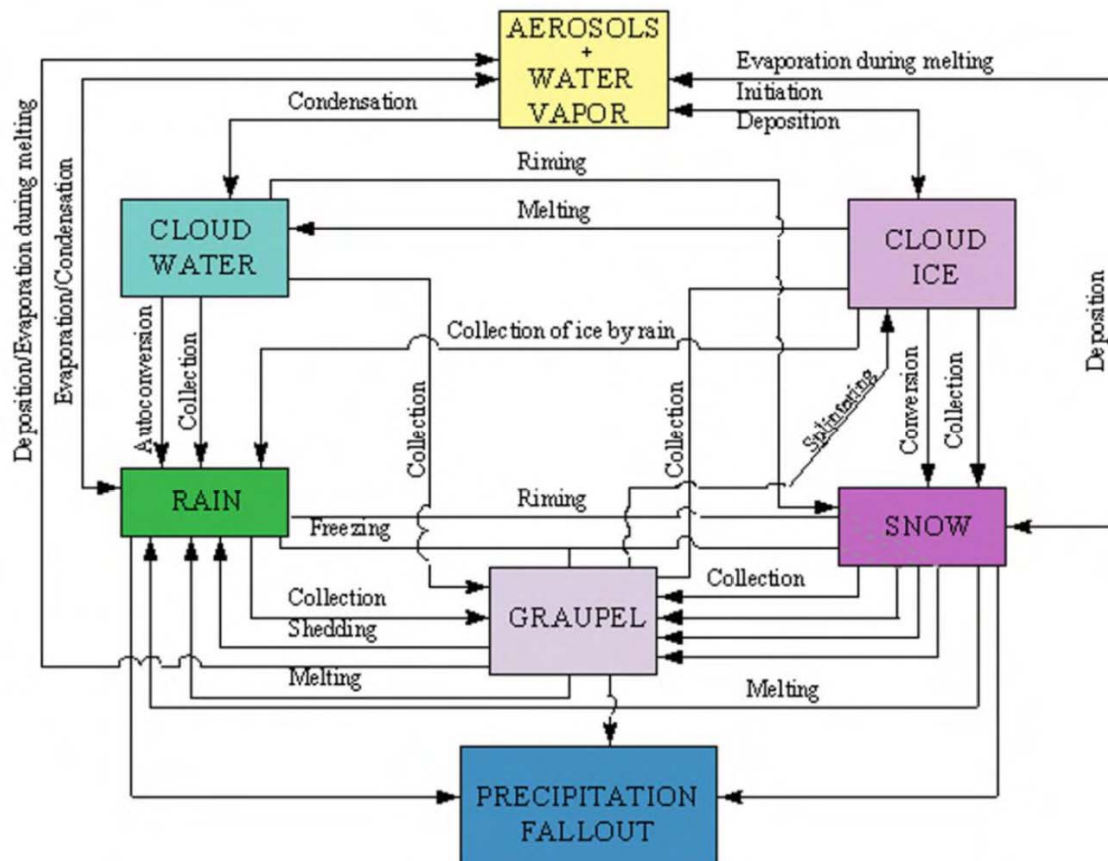


Figure 2.2: Mixed phase microphysical processes in a cloud (Houze 1993)

In order to enhance precipitation, the concept of seeding is to seed with appropriate CCN (Cloud Condensation Nuclei) or IN (Ice Nuclei) to make precipitation develop more efficiently.

Mixed-phase/ice processes initiated by freezing of large drizzle/rain drops and subsequent initiation of natural seeding (ice splintering) process rapidly depleting cloud liquid water content. In this respect, following processes are important to be considered

- Large drop freezing at $\sim -5^{\circ}\text{C}$
- Initiation of ice splintering process
- Rapid conversion of LWC (Liquid Water Content) to ice
- Rapid depletion of LWC inhibiting lightning in these cases

Hygroscopic seeding

Hygroscopic seeding is defined according to the National Academies report as ‘to enhance rainfall by seeding clouds with appropriately sized salt particles or droplets, promoting the coalescence process. *The intention is to promote particle growth through coalescence and thereby improve the efficiency of the rainfall formation process. And is through following processes,*

- **Large hygroscopic particle seeding**, which seeds clouds with large salt particles (e.g., $>10\ \mu\text{m}$ dry diameter) to short-circuit the condensation growth process and provide immediate raindrop embryos to start the coalescence process. Examples: Project Cloud Catcher, India, Thailand.
- **Hygroscopic flare seeding**, which focuses on broadening the initial drop spectrum during the nucleation process by seeding with larger than natural CCN ($0.5\ \mu\text{m}$ to $3\ \mu\text{m}$ dry diameter) to enhance the coalescence process in warm and mixed-phase clouds. Examples: South Africa, Mexico experiments.

A conceptual understanding on Hygroscopic seeding is illustrated in Figure 2.3. The hygroscopic nuclei dispersed at the cloud base produces larger cloud droplets than present in a developing cloud, leading to collision coalescence and that accelerates rain formation. Since its inception, the term “hygroscopic seeding” has taken on slightly different meanings depending on the experimental design, type of seeding material used, and the type of cloud that was the subject for experimentation.

In all instances the ultimate goal has been to enhance rainfall by somehow promoting the coalescence process. The direct introduction of “appropriately” sized CCN that can act as artificial rain drop embryos using either water sprays, dilute saline solutions, or grinded salts, are the most common hygroscopic seeding techniques used previously.

The primary objective of introducing artificial rain drop embryos (salt particles larger than 10 microns diameter) is to short circuit the action of the CCN population in determining the initial character of the cloud droplet population, and thus, jumpstart the coalescence process.

Precipitation development: Precipitation formation in convective clouds may be dominated either by coalescence processes or ice-phase processes. Storms with high droplet concentrations of small sizes tend to be dominated by ice-phase processes. The result is a large number of small ice particles, many of which fail to reach the ground and either evaporate or enter the anvil cloud.

Results from the South African, Mexican and Australian experiments indicate that hygroscopic seeding at cloud base early in cloud development may significantly increase the rainfall from continental storms. The hygroscopic flares provide larger CCN than naturally occurs which activate at lower super saturations, condense water more readily and tend to limit the total number of droplets activated. The resulting droplets grow to larger-than-normal sizes through condensation, and then rapidly grow further through collision with other droplets within 15-min (Cooper et al. 1997), initiating the rain process within the convective cell.

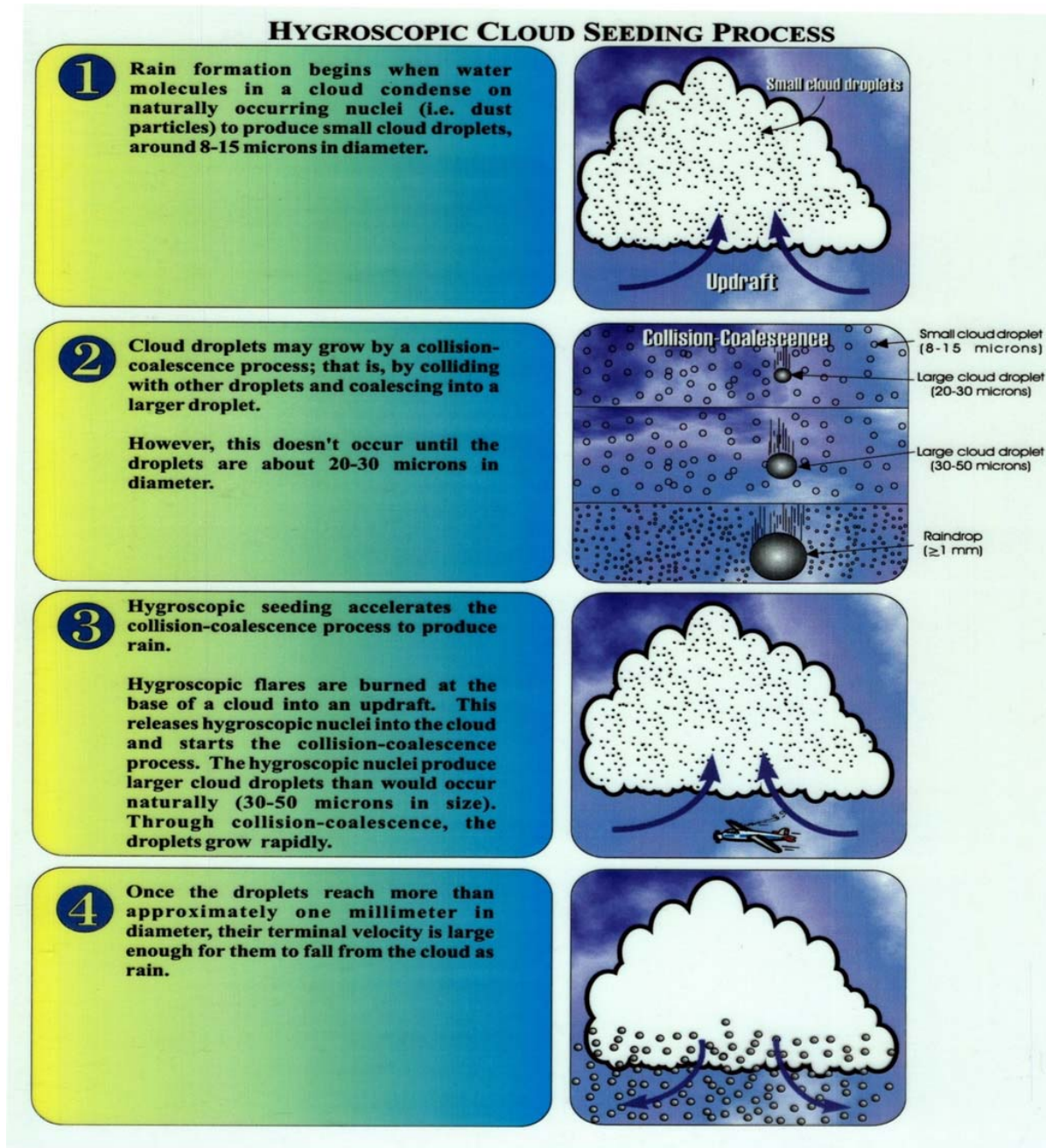


Figure 2.3: Conceptual understanding on the hygroscopic seeding

Background: South African experiment developed use of flares for hygroscopic seeding; 5-year randomized experiment (127 cases) and illustrated dramatic results using individual storms as the experimental unit. Radar derived rainfall estimates indicated that rainfall was significantly ($\approx 40\%$) increased cloud systems that were seeded.

In another example of 1995 Arizona Project, case study of seeding a (wintertime) convective cloud; used chaff as a tracer (X-band radar) and Ka-band radar to detect seeding signature (regions of enhanced reflectivity).

1996 Mexican State of Coahuila: Found similar results to the South African results.

The common elements of the three randomized experiments were:

1. Seeding with hygroscopic particles
2. Evaluation using a time-resolved estimate of storm rainfall based on radar measurements in conjunction with an objective software package for tracking individual storms (different software was used for each experiment), and
3. Statistically significant increases in radar-estimated rainfall.

The Mexico experiment was designed to replicate, if possible, the South Africa experiment, and employed end-burning flares to dispense the seeding agent. The results were found to be remarkably consistent. Increases in target cloud radar-estimated rainfall were deduced in the period 30-60 min after seeding in both cases (a somewhat later time period than might have been expected).

All these experiments illustrated that understanding and documenting the physical chain of events (microphysical and dynamical responses) remains an important step toward acceptance of the statistical results.

The physical hypothesis for these experiments was based on the static-mode seeding concept, or seeding for microphysical effects. The hygroscopic particles would act to increase the efficiency of the rain formation process by accelerating the condensation–coalescence–collision process in the cloud. In the South Africa and Mexico experiments **cloud condensation nuclei was introduced in to the cloud to affect the condensation process by broadening the initial cloud drop size spectrum**, there by promoting the competition effect. Meanwhile in the Thailand and India experiments **ultra giant condensation nuclei (UGCCN) was introduced into the cloud to fasten the collision–coalescence process**. It is understood that both approaches would promote the earlier development of precipitation particles and increase available cloud water content leading to rain formation, which may be more than the ones occur through natural process.

In both the South Africa and Mexico experiments, the statistical results could be physically explained by the microphysical seeding hypothesis until about 30 min after decision time but could not explain the apparent seeding effect beyond 30 min. This might indicate a **dynamic response in the cloud system that carries the effects of seeding beyond the initial production of precipitation**.

It is emphasized that the physical evaluation criteria be based on physical observations taken as an integral part of the randomized experiment in order to verify pivotal links in the chain of physical events associated with the seeding conceptual model

‘The AMS (American Meteorological Society) Policy Statement on Weather Modification (AMS 1998) **called for both statistical and physical evidence as proof of the success of any cloud seeding experiment. The establishment of unambiguous, objective physical evaluation criteria is needed to confirm that the effects of seeding suggested by results of the statistical experiment were likely caused by the seeding intervention, that is, that the physical evidence is consistent with the statistical evidence.**’

Indian cloud seeding experiment (Murthy et al 2000) concluded that the seeded clouds had an advantage in the initial development of precipitation-size drops in accordance with the seeding hypothesis. The liquid water content and updraft velocities were higher in the seeded clouds. Murthy (2000) indicated this as physical evidence in support of the possibility that the hygroscopic particle seeding was accelerating the condensation–coalescence process, in accordance with the seeding hypothesis.

WMO (World Meteorological Organization) report of the Weather Modification Research (2010) indicates that ‘continuing strategic research is required to investigate and explain the scientific hypotheses on which weather modification is based. ***Because this research is inherently focused on important atmospheric processes, it is relevant not only to weather modification but also to the improvement of weather and climate prediction that supports a wide range of applications such as water management and climate change adaptation.***’

First step in a cloud seeding program is to develop a data base on the following

- Climatology of clouds and precipitation in a region
- Thermodynamic and wind structure of the atmosphere
- Aerosol and associated microphysical variations

WMO recommendations (2010) indicate that, to increase the chances of success in a specific situation, it should be verified through preliminary studies that:

- (a) The climatology of clouds and precipitation at the site indicates the possibility of amenable conditions for weather modification;*
- (b) Conditions are suitable for the available modification techniques;*
- (c) Modelling studies support the proposed weather modification hypothesis;*
- (d) Socio-economic and environmental consideration should be included as an integral part of the design of weather modification research experiments and operational programmes.*

WMO recommends that cloud seeding projects for precipitation modification be designed to allow statistical and physical evaluation of the results of seeding.

Following steps are to be undertaken as part of physical studies

- Determine conditions and locations favorable for convective development and document subsequent evolution of convective clouds.
- Characterize the CCN spectrum and its variability over the range of these convective conditions.
- Determine the primary precipitation mechanism and the natural variables that change or modify it.
- Document microphysical signatures, such as cloud droplet distribution, drop formation, or echo development, in seeded clouds.
- The characterization of the seeding material.

Components of field project

- Surface rainguage network
- Automatic weather stations
- Aircraft
- Upper air radiosonde unit (a Microwave Radiometer can give detailed continuous thermodynamic development of the cloud)
- Radar
- Thunderstorm Identification, Tracking, Analyses and Nowcasting (TITAN)
- Collision coalescence modeling

Confirmatory experiment (based on South African experiment):

- Double-blind randomization
- Seeding with hygroscopic flares
- Evaluation based on time-resolved radar-rainfall
- estimates from objective TITAN software

Time series variables

- Radar-estimated precipitation flux ($\text{m}^3 \text{s}^{-1}$), using the Marshall-Palmer Z-R relationship
- Total storm mass (in kilotons).
- Storm mass above 6 km MSL (in kilo tons).
- Storm area (km^2).
- (Height of maximum reflectivity) - (Z-weighted vertical centroid)

Storm (time-integrated) Variables

- Total case precipitation in kilotons from decision time until 60 minutes after decision time.
- Area-time-integral (ATI) is given in km^2h from decision time until 60 minutes after the decision time. (ATI is defined as the integral of storm area over time, computed using discrete volume-scan time intervals.)
- Duration of the experimental unit from decision time to 60 min after decision time and a list of Radar derived parameters are given in Table 2.1.

Table 2.1 Radar derived storm parameters

Storm track characteristic	0.10th quantile	Median	0.90th quantile
Duration (hr)	0.3	0.6	1.4
Mean volume (km ³)	26.2	53.5	180.4
Maximum volume (km ³)	35.9	86.5	356.1
Mean area (km ²)	13.4	23.2	58.7
Maximum area (km ²)	18.0	34.9	106.9
Mean cloud top height (km)	6.0	7.8	10.2
Max cloud top height (km)	6.1	9.1	12.9
Mean reflectivity (dBZ)	35.0	38.6	41.4
Maximum reflectivity (dBZ)	43.5	51.5	58.5
Rain volume (m ³)	52,842	197,597	1,501,110

Hygroscopic seeding Hypothesis and procedures: The seeding material is dispersed into the inflow region at cloud base. Because these particles are larger and more hygroscopic than the natural particles, cloud droplets will nucleate preferentially on the seeding particles. This inhibits a portion of the smaller natural cloud condensation nuclei from becoming activated because the maximum super saturation is limited by the droplets already formed as a result of seeding. The result is a broader-than-natural droplet spectrum near cloud base that enhances the potential for precipitation to develop earlier and more efficiently in the lifetime of the cloud. In addition, the expectation is that this seeding effect will spread to other parts of the cloud and enhance the formation of precipitation there (if updrafts are greater than 200 ft/min). The ultimate effect is a more efficient precipitation process. For hygroscopic flare seeding Figure 2.1 provides an overview of the selection criteria and hypothesis.

The objectives of each operation will be to select suitable candidate storms, randomly seed them and make the measurements that are required to detect and analyze any seeding effects.

Seeding will be carried out in a randomized manner, following the procedure used in the experiment. This process is necessary to allow a rigorous statistical analysis of the seeding effects. Since the radar operator is unaware whether seeding is actually being performed or not, the pilot will fly the mission in exactly the same manner irrespective of the random seed/no-seed decision. After decision time on any case the radar operator will not provide the pilot with any information on how the storm is responding to the seeding event.

Hygroscopic Conceptual Model

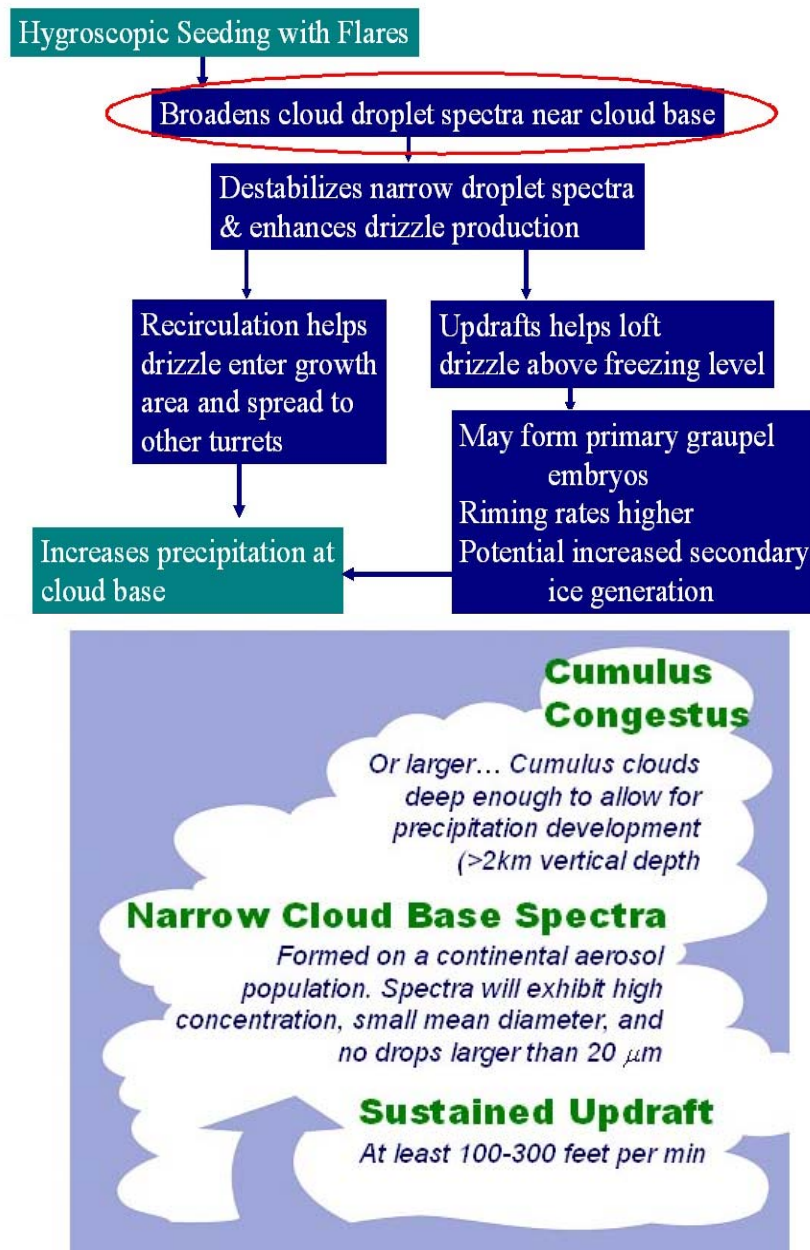


Figure 2.4: Hygroscopic seeding conceptual model and criteria for candidate clouds (Source Bruintjes).

Area of operation: An area between the three corners of a triangle; Hyderabad, Begumpet airport (17°13'47.71"N, 78°28'14.61"E), Anantapur (14°40'45.1"N, 77°36'12.68"E) and Solapur (17°40'28.09"N, 75 °54'44.37" E) is considered. The main area of operation is given in Figure 2.5. The radar location is approximately 95.3 km from CAIPEEX base at Begum Peth airport. The ground observation site is approximately 100 km from the base.

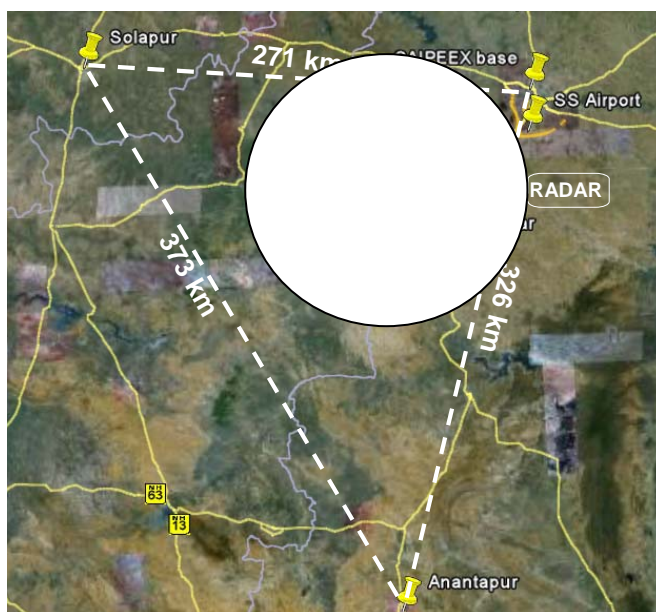


Figure 2.5: The area of operation

Flight plan and decision procedure: Each morning, a radiosonde was launched at 10 AM. To obtain a sounding of local atmospheric conditions from the ground site of CAIPEEX Integrated Ground Observation Campaign (IGOC) at Mahabubnagar. A radiometer positioned at IGOC site using RAOB (RAwinsonde OBservation) was very useful in updating the thermodynamic characteristics and growth of the boundary layer and residual layer breakup. In addition, the operation base was acquiring meteorological data from web sites at IITM, (IMD), and National Center for Medium Range Weather Forecast center (NCMRWF) to assist with the forecasts. CAIPEEX Convective Potential Forecast Model (CCPFM) was giving daily forecast at 3 km resolution at hourly intervals for producing the area specific and product specific forecasts for the operational decisions. A weather brief and flight plan protocol was formulated and followed on each day for the decision making relating to the flight plan the kind of flight missions to accomplish for that day.

Hygroscopic Burn-in-Place (HBIPs) flares are used in the experiment: To enhance collision-coalescence processes through development of large cloud droplets. A flare comprised of KCl (Potassium Chloride) and NaCl (Sodium Chloride) and has a burn time of approximately 4 minutes. Pairs of flairs are burned and a total of 8 flares (4 burns x 2 per burn) per event is burned which takes 16 minutes. Up to 3 seeding events are carried out per flight

Once the decision is taken to have a flight with randomized cloud seeding objective, the seeder aircraft is sent out for a survey. The research aircraft takes off after hearing from the seeder aircraft about the cloud survey over the region about developing convection, which may not have registered within the C-band radar echoes. Prior to starting the seeding, the research aircraft measured the natural aerosol size distribution and CCN entering cloud base by performing an elongated racetrack pattern approximately 1000 ft below cloud base. This takes approximately 15 minutes, depending on the CCN cycle (CCN measurements at different super saturation settings). During this time, the seeding aircraft looked for suitable updrafts. Once the below cloud aerosol measurements are completed, the cloud base measurement phase was completed.

A measurement of cloud base (height, pressure, and temperature) is obtained with the seeder aircraft flying straight and level at cloud base without penetrating any cloud. After the cloud base measurements the research aircraft ascend to 1000 ft above cloud base and conducted a penetration in an actively growing convective cloud.

The radar scientist guides the pilot to the most promising storms. Until decision time the radar scientist and pilot converse about the nature of the situation about choosing a storm. The pilot searches visually for a suitable candidate storm in the area. This storm must have a solid-looking at least 2 km in diameter base with a good updraft ($>200\text{ft/min}$ as measured by the aircraft flying through the updraft) as well as the appearance of growth (with cauliflower like bright tops). The pilot will determine whether the location of the storm relative to terrain is suitable for seeding (High enough above the terrain to conduct safe cloud seeding at the base). The radar operator will determine if the storm is located appropriately for good radar coverage (between 10 and 110 km range). If a case moves outside of this range, it will be discarded. When the pilot decides that a case has been found, he/she will declare that information to the radar. This time is referred to as ‘decision time’.

Randomization procedure: CAIPEEX project used the same randomization procedure as that used in the South African, Mexican and Australian experiments.

Two sets of decision envelopes were made, one at the radar and one in the aircraft. This procedure was followed to ensure that none of the project personnel has prior knowledge of the contents of the envelopes. The radar envelopes contain either a ‘seed’ or a ‘no-seed’ decision. The aircraft envelopes contain either a ‘yes’ or a ‘no’ decision.

Once the pilot has declared a ‘case’, both the radar operator and the pilot open the next envelope in each sequence. The radar operator communicates the result from the radar envelope to the pilot, who then decides whether to seed or not based upon the following decision table:

<u>Radar</u>	<u>Aircraft</u>	<u>Action</u>
seed	no	no-seed
seed	yes	seed
no-seed	yes	no-seed
no-seed	no	seed

The pilot will not tell the radar operator whether the decision is to seed or not, and the pilot and radar operator will not communicate on issues related to the effects of seeding or lack thereof.

Seeding procedure: If the decision is to seed, the pilot will burn 2 flares at a time, one on each wing, while flying below cloud base and through the updraft as much as is possible. A maximum of 8 flares is to be used on any one case, leaving 8 flares for a possible second case. The flares take approximately 4 minutes each to burn completely, therefore the maximum seeding time will be 16 min per case.

Ideally, flares should be burned continuously, starting new ones as the previous pair burn out. However, the pilot may choose to suspend seeding in order to fly away from the storm and perhaps gain altitude to get a clear picture of the position of the new development. Therefore a case may last longer than the 16 minutes of flare burn time. If the situation deteriorates to the point at which seeding is not considered effective, (i.e. when the updraft ceases or becomes poorly defined) seeding is terminated.

If the decision is no-seed, the pilot fly the mission in exactly the same manner as if the decision were for seeding, up to a maximum seeding time of 5 min. This includes breaking off the mission should the seeding situation become unfavorable. The pilot will record flare burn times. The pilot should note start and end times for seeding. Table 1 gives a list of randomization cases carried out with both aircrafts during CAIPEEX-2011 campaign.

Table 2.2 List of randomized cases during CAIPEEX 2011 experiment

Aircraft	Case nr	Date	Start time	End Time	Latitude	Longitude
ZJRA	1	27/10/2011	10:52:00	11:02:00	16.7263	77.0641
ZJRA	2	27/10/2011	11:49:30	11:54:00	17.1399	77.8306
ZJRA	3	28/10/2011	7:25:30	7:30:30	16.2210	77.5465
ZJRA	4	28/10/2011	9:41:41	9:51:41	16.1662	78.1414
ZJRA	5	31/10/2011	10:05:10	10:10:10	16.5575	78.9686
ZJRA	6	01/11/2011	8:48:00	8:58:00	16.1081	78.3295
ZOCP	1	02/10/2011	8:38:00	8:43:00	17.4366	78.6057
ZOCP	2	02/10/2011	8:45:00	8:54:00	17.4900	78.6009
ZOCP	3	02/10/2011	9:39:00	9:45:00	17.3610	77.8967
ZOCP	4	03/10/2011	8:50:00	9:05:00	16.4775	77.6686
ZOCP	5	03/10/2011	9:28:00	9:32:00	16.3804	77.2273
ZOCP	6	05/10/2011	10:25:00	10:29:00	16.5959	77.1790
ZOCP	7	08/10/2011	8:37:00	8:45:00	16.6200	78.1100
ZOCP	8	08/10/2011	9:17:00	9:27:00	16.5791	77.2695
ZOCP	9	25/10/2011	10:28:30	10:38:00	16.3432	77.8960
ZOCP	10	25/10/2011	11:04:30	11:13:10	16.7700	78.0009
ZOCP	11	26/10/2011	8:19:10	8:23:30	16.8880	78.0405
ZOCP	12	26/10/2011	8:35:40	8:40:00	16.8860	77.6979
ZOCP	13	26/10/2011	8:46:00	8:50:00	16.5300	77.3700
ZOCP	14	27/10/2011	8:18:00	8:27:00	16.4950	77.7348
ZOCP	15	28/10/2011	9:19:40	9:22:00	16.2218	78.1949
ZOCP	17	28/10/2011	7:19:18	7:26:00	16.4450	77.7277
ZOCP	19	28/10/2011	7:20:30	7:25:30	16.1929	77.7959
ZOCP	20	31/10/2011	9:12:00	9:18:00	16.3124	78.6369
ZOCP	21	31/10/2011	9:38:10	9:42:00	16.2433	78.3357
ZOCP	22	31/10/2011	10:13:05	10:19:00	16.3506	77.9542

The radar data was analyzed using TITAN storm tracking software (Dixon and Wiener, 1993). This software identifies storms in a volume scan as those contiguous regions which exceed a given reflectivity threshold. In the analysis, the threshold was set to 30 dBZ.

Response variables for analysis of seeding

Results from the South African, Mexican and Australian experiments point to increases in certain response variables in the period from 20 to 50 minutes after decision time.

Therefore, CAIPEEX consider time series of the following quantities as response variables:

1. Radar-estimated precipitation flux. Precipitation flux will be estimated using the Marshall-Palmer Z-R relationship applied to a composite of the maximum reflectivity's at any height in the storm. The composite technique will be used to minimize range bias.
2. Total storm mass, where storm mass (in ktons) is computed using the relationship $m = 20300 Z^{1.67}$, where m is in $g\ m^{-3}$ and Z is the radar reflectivity factor in $mm^6\ m^{-3}$.
3. Storm mass (computed as for item 2) above 6 km MSL.
4. Storm area.
5. Height of maximum reflectivity
6. (Height of maximum reflectivity) - (Z-weighted vertical centroid).

The nature of the response over time will be used to either confirm or discard the validity of the seeding hypothesis.

In addition, the following quantities will be considered response variables:

1. Total case precipitation from decision time until 60 minutes after decision time.
2. ATI from decision time until 60 minutes after decision time. ATI is defined as the integral of storm area over time, computed using discrete volume-scan time intervals.
3. Duration of the experimental unit from decision time to a maximum of 60 min after decision time.

Statistical hypotheses

The following hypothesis will be tested for each time series response variable:

Seeded cases will demonstrate an increase in response quantity over the unseeded cases during the time period 10 to 60 minutes from decision time.

The following hypothesis will be tested for the other response variables:

Seeded cases will demonstrate an increase in the response quantity over unseeded cases.

The null hypothesis is that there will be no differences in the response variables for the seeded and unseeded cases.

Statistical evaluation

The time series response variables will be tested using the 0.25th, 0.50th, and 0.75th quantiles (i.e., first three quartiles) of the distributions of the values of the variables for seeded and unseeded cases. These variables will be measured at 5 minute intervals from 10 to 60 minutes from decision time.

Several statistical techniques can be used including a re-randomization technique to test the statistical significance of the differences in the 0.25th, 0.50th and 0.75th quantiles of the time series response variables for the seeded and unseeded cases at the specified times. These tests will be one-tailed tests at the 0.05 level, testing the alternative hypotheses of increases in the response variables for the seeded storms. Exact probability values will also be computed for each test. Differences in other response variables also will be tested using the re-randomization technique.

The re-randomization procedure is the same as the procedure used to evaluate results of the South African, Mexican and Australian experiments (Mather et al., 1997; WMO; 2000, Tessendorf et al. 2011). Other exploratory analyses may be undertaken, but the re-randomization tests will be the basis for evaluation of the success of the experiment. Sample evaluations of the cases from CAIPEEX 2011 are depicted in Figure 2.6.

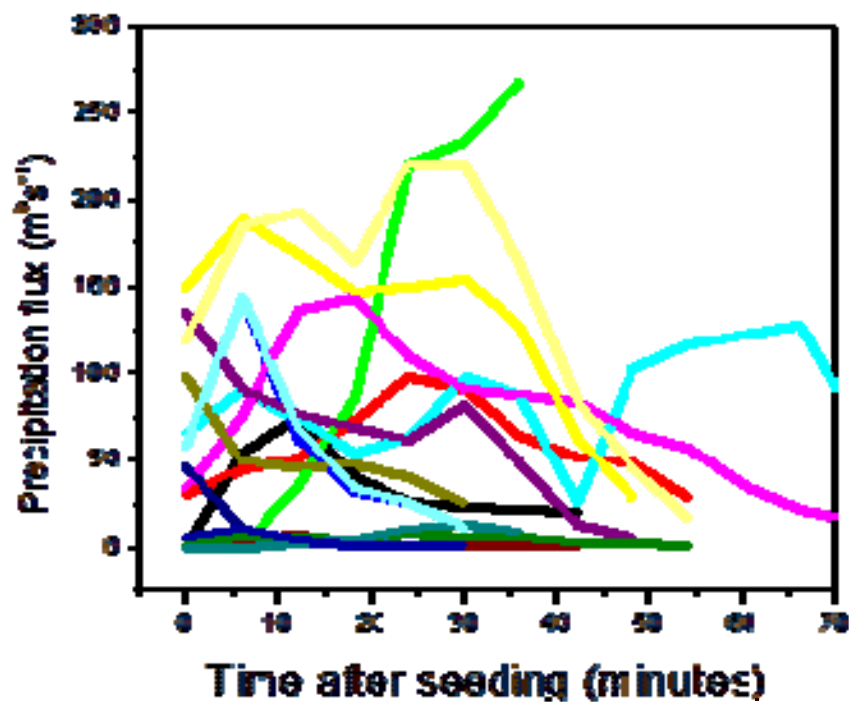


Figure 2.6: Precipitation flux from 10 randomized cases from Table 2.2

Future directions:

The randomized cases collected during the CAIPEEX 2011 experiment is not enough to draw any statistics on the outcome of randomized seeding as illustrated. This requires more samples and further systematic studies with advanced methods such as dual Doppler radars, to investigate the dynamical response to the seeding.

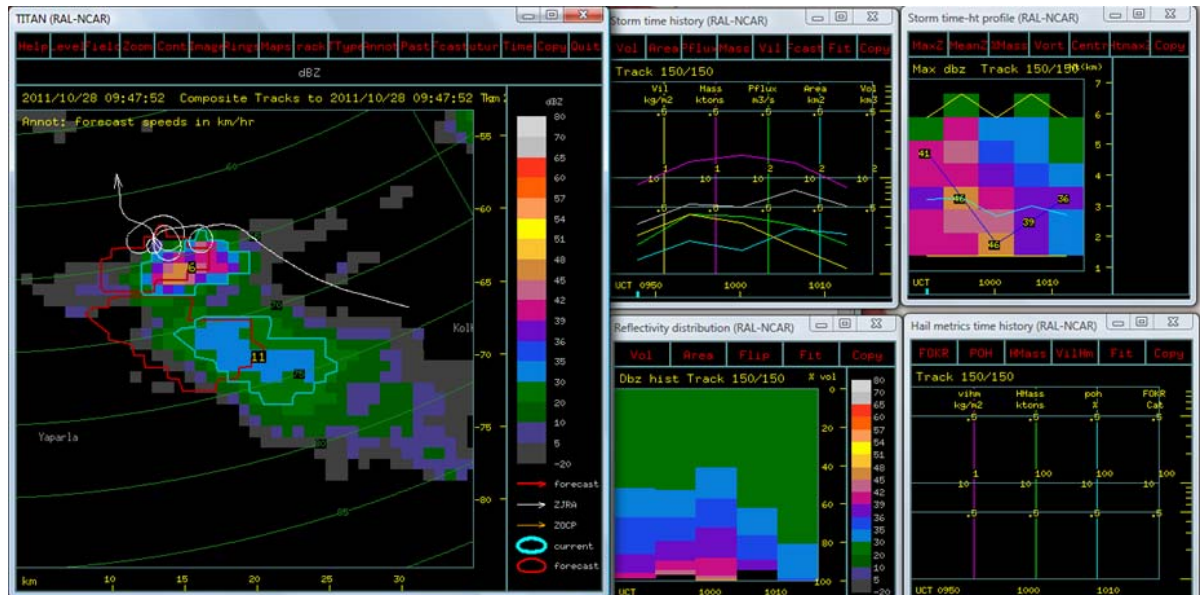
Report of National academies emphasizes the need to improve cloud model treatment of cloud and precipitation physics by stating that ‘Special focus is needed on modeling CCN, ice nuclei processes, and the growth, collision, breakup, and coalescence of water drops and ice particles. Such studies must be based on cloud physics laboratory measurements, tested and tuned in model studies, and validated by in situ and ground observations.’

References

- Mather, G.K., Terblanche, D.E., Steffens, F.E. and Fletcher, L., 1997: Results of the South African cloudseeding experiments using hygroscopic flares, *J. Appl. Meteor.*, 36, 1433–1447.
- Tessendorf, S.A., Weeks, C.E., Brintjes, R.T. and Axisa, D., 2011: Cloud base aerosol characteristics and implications for cloud microphysics in Southeast Queensland. Preprints, 18th Conf. Planned and Inadvertent Weather Modification, Amer. Meteor. Soc., Seattle, WA.
- Dixon, M.G., Wiener, 1993: TITAN: Thunderstorm Identification, Tracking, Analysis, and Nowcasting—A Radar-based Methodology, *J. Atmos. Oceanic Technol.*, 10, 785–797.
- Murty, et al. 2000: 11-year warm cloud seeding experiments in Maharashtra, India. *J. Wea. Modif.*, 32, 10-20.
- Houze, R.A., Jr., 1993: *Cloud Dynamics*. Academic Press, San Diego, 573 pp.

Theme 3

Radar data analysis with TITAN



A CAIPEEX case of seeding is viewed in TITAN

Contributors: Murugavel, Manoj, Gayatri, Sachin, Neelam, Resmi, Roelof Burger, Roelf B., T. Prabhakaran

TITAN Thunderstorm Identification Tracking Analysis and Nowcasting

TITAN can be downloaded from

http://www.ral.ucar.edu/projects/titan/download/titan_licence.html

<ftp://ftp.rap.ucar.edu/pub/titan/distribution/>

Install the newest version from that directory

Installation guide is available at

<http://www.ral.ucar.edu/projects/titan/docs/TitanInstall.pdf>

The TITAN installation need tcsh shell

LINUX is the only fully-supported platform for running TITAN.

Make a username titan5

Create user for titan5 and install titan5 software. This will create "rap" directory containing all programs.

Hardware specifications

- CPU - 3.0+ GHz. For real-time (and especially time-series work), fast quad-core processors are recommended.
- RAM - 2 to 8 GBytes

Disk space: large disks are good for archiving data. At a minimum, you should have a 200 Gbyte disk for a real-time system. For data archival, 500 GByte to 1 TByte is good.

- Graphics card: 256+ MByte memory for 1600x1200 screen resolution.
- Check for LINUX compatibility. For specific hardware devices, it is worth checking, via Google searches, that a good driver is available.

Common TITAN commands

Start Rview to display data

1. Copy projDir to /home/titan5
2. Goto /home/titan5/projDir/display/params directory.
3. Type Rview -params Rview.ops
4. If Rview.ops does not exist, then generate with Rview -print_params > Rview.ops
5. Navigate with time, field etc.

Almost all TITAN applications conform to three conventions on command line arguments, ‘-h’, ‘-print-params’ and ‘-params’

- -h: get help, or print the usage.
- -params: specifies which parameter file to use for running the application.
- -print_params: print a default version of the parameter file to stdout.
- cd /home/titan5/projDir/display/params
- Rview -params Rview.ops

TITAN Installation

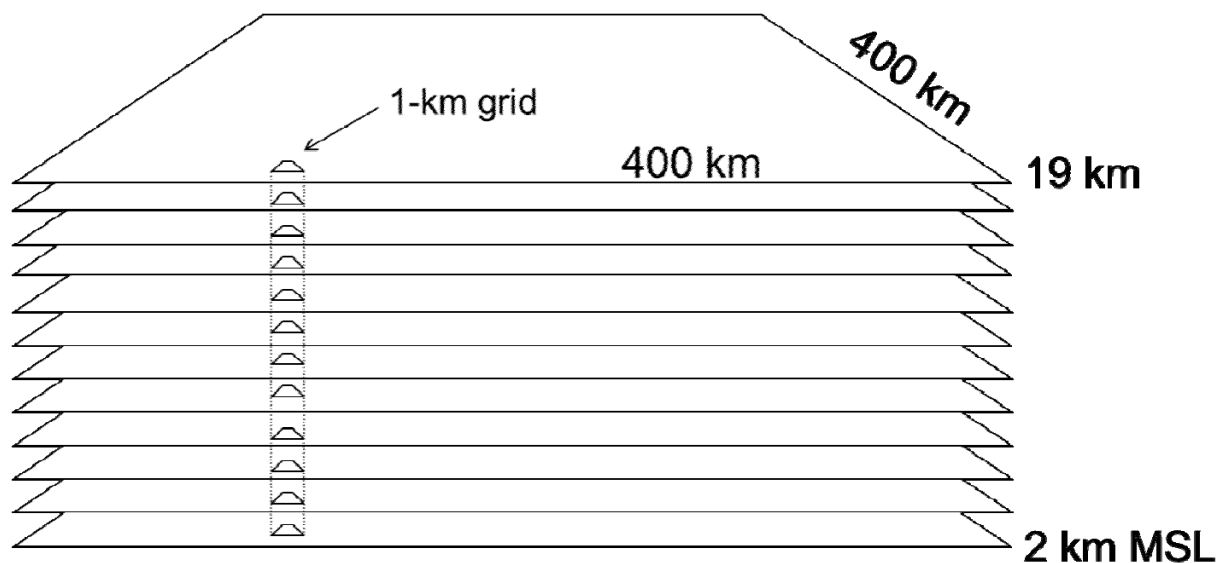
```
cd projects/titan5/projDir/display/params
./set_build_env
./clean_titan_build
./set_titan_env -64
cd titan
./install_cshrc
source ~/.cshrc
./set_build_env -64
./build_titan
cd ~/rap/projects/ticd ~#+1298459776
tcsh
echo $SHELL
echo $RADAR_LAT
echo $RADAR_LON
echo $RVIEW_MAP_CONF_FILE
cd home/titan5/projDir/data/$RADAR_CART_DIR
Titan -print_params >Titan.archive
echo $DATA_DIR/RADAR_STORMS_DIR
input: “$(DATA_DIR/$RADAR_CART_DIR)”
output: storm_data_dir= “/home/titan5/projDir/data/titan/storms”
```

Get telemetry data

```
scp pmvelu@10.2.6.53:caipeex2011-telemetry.tgz /home/titan5
cd home/projDir/data/titan/storms
cd titan5/RadarConfig/Bubnagar/anal
source .cshrc
cd projDir/data/logscd projDir#+1298460068
cd projDir/data/
/bin/rm -rf save.*
cd rap/projects/titan
cd rap/projects/titan/templates/tem#+1298460156
cd templates/
cd template_single_rcd tem#+1298460171
./INSTALL_TITAN
cd projDir/data/sim/c#+129846019cdcd projDir/data/sim/
cd rap/projects/titan/templates/template_single_radar/sy#+1298542730
mv projDir projDir-tsu
mv projDir projDir-template
ln -s projDir-sur projDir
ls $RAP_DATA_DIR/mdv/radar/###+1298543133cls
```

Data

TITAN data is in a gridded domain as illustrated in Figure 3.1. There are different data formats in Titan (Table 3.1) with various applications. The mdv (meteorological data volume) format is used to save CAIPEEX C-band radar data. Mdv is used for gridded data, which is representing the data volume and each dataset is saved in separate files, the data and time could be indicated in the filename itself. Data could be viewed with different thresholds in the identification of cells and also can display information from all altitudes projected to the surface as a composite reflectivity.



Domain = 400 km x 400 km x 18 km

Figure 3.1: TITAN gridded domain

Table 3.1 Data formats in Titan

raw	Data in whatever format it is in when received from the outside world
fmq	(File Message Queue) Circular queue used for ingesting beam data in a common format
mdv	(Meteorological Data Volume) Format used for storing gridded data within the system
titan	Format of storm data as output by Titan algorithm
spdb	(Symbolic Product DataBase) Format used for storing non-gridded data within the system

(RAP dataset paths always given relative to \$RAP_DATA_DIR)

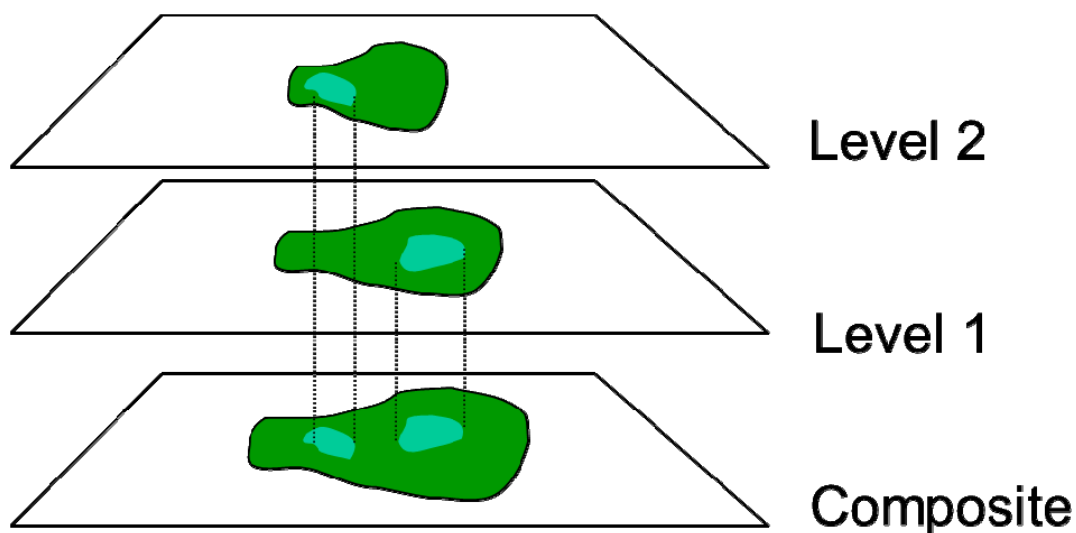


Figure 3.2: Viewing composite reflectivity

Data view

Clutter removal: Using the identifying characteristics of clutter, automated data processing can recognize conditions where clutter is most common.

Important parameters for identification are:

- Consistent and well-calibrated reflectivity data (returned radar power).
- Accurate Doppler velocity.
- Strong Doppler signal strength for determining velocity spectrum width.
- Continuous data (no “missing beams”).

However, even with ideal data, the nature of all radar returns cannot be determined unambiguously. Any automated process should error on the side of keeping some clutter rather than eliminating real weather echoes

Useful parameters from TITAN

Vertically integrated liquid (VIL) and precipitation flux are useful parameter derived from TITAN analysis. The schematic diagram (Figure 3.3 and 3.4) shows the method of estimation of VIL and P flux from a single cloud through TITAN. Similarly we can also estimate maximum dBZ, mass, volume, area for each storm with track number and complex numbers.

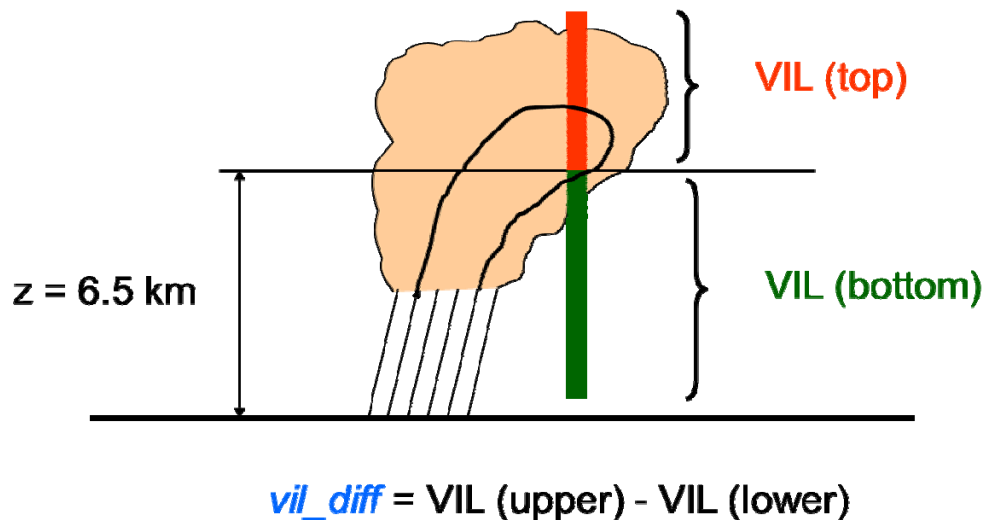


Figure 3.3: Illustrates the vertically integrated flux from the upper and lower part of the cloud which could be estimated using TITAN

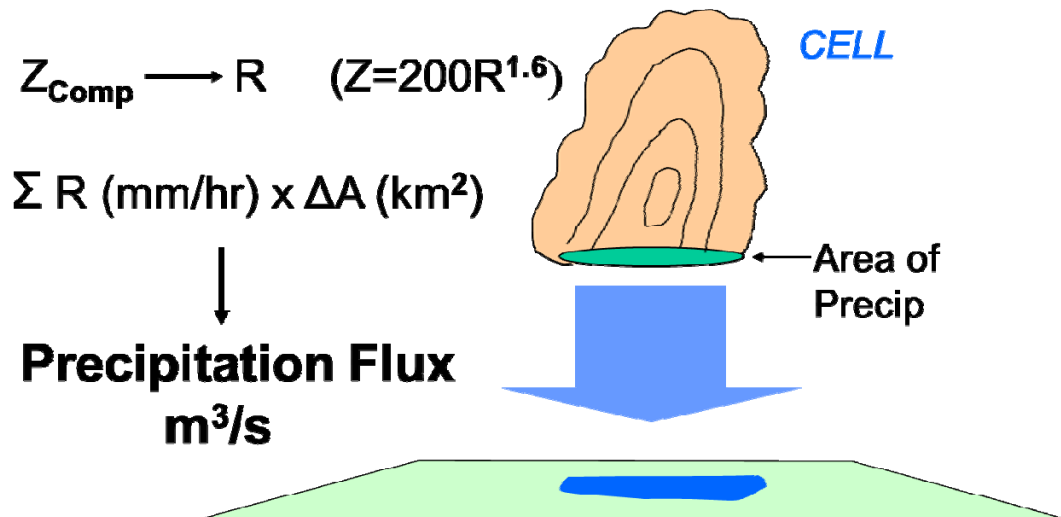


Figure 3.4: Illustrates the precipitation flux from TITAN

Tracking and Statistical Information

Storm Tracking

1. Goto /home/titan5/projDir/titan/params directory.
2. Check Titan.archive file.
3. If it doesnot exist, create it by "Titan -print_params > Titan.archive
Tracks2Ascii -print -params > Tracks2Ascii.caipeex

Tracks2Ascii -print -params > Tracks2Ascii.caipeex -start "2011 09 21 0 0 0" -end "2011 11 11 23 59 59"

4. Review this file to change various parameters like input_url (data input), storm_data_dir (output data), low_dbz_threshold (threshold dbz for considering storm) etc. and change accordingly, if required.

5. Execute Titan -params Titan.archive -start "2011 09 21 0 0 0" -end "2011 11 09 23 59 59"
6. This will create /home/titan5/projDir/data/titan/storms directory containing 4 files for each day.
7. Now Rview GUI will show storm information.
8. Rename this directory before running this program for another set of parameters. COMPLETE TRACK -> Statistics for all files

Tracks2Ascii is used to derive all track statistics

1. This utility produce tracks data in ascii format for each storm
2. Goto /home/titan5/projDir/anal directory
3. Generate parameter file by using "Tracks2Ascii -print_params > Tracks2Ascii.caipeex"
4. And then execute "Tracks2Ascii -params Tracks2Ascii.caipeex -start "2011 09 21 0 0 0" -end "2011 11 09 23 59 59" > tracks1.txt"
5. Now the tracks1.txt file will contain all the track information. Identify them by storm number, date, time alongwith other characteristics.
6. Use this data file with excel/origin/matlab to separate the columns and statistics on individual cases.

Edit Track2Ascii.caipeex by changing the following:

target_entity=TRACK-ENTRY

sample_interval=-1 (for every volume scan)

Ingesting telemetry data

store telemetry data in ~/projDir/ingest/params

EsdAcIngest.tgz

tar -zxvf EsdAcIngest.tgz

1. Type "EsdAcIngest -print_params > EsdAcIngest.archive" to create parameter setup file
2. Open this file and change the parameters as you required, e.g.,
 1. mode=ARCHIVE
 2. input_format=AUTOMATIC_FORMAT
 3. output_url=/home/titan5/projDir/data/spdb/ac_posn
 4. output_ascii=FALSE and etc.
4. run EsdAcIngest -params -verbose EsdAcIngest.archive
5. o/p of this will be stored at /home/titan5/projDir/data/spdb/ac_posn directory
6. Now in the Rview.ops file, incorporate this directory in the display fields links
7. Now you can see the a/c tracks in Rview.


```
EsdAcIngest -print -params > EsdAcIngest.archive
```

Edit “EsdAcIngest.archive” and make changes as below and save it:

```
Mode =ARCHIVE
```

```
REALTIME -> ARCHIVE
```

```
Input-format=AUTOMATIC
```

```
Check
```

```
Input devices = for realtime mode
```

```
callsign =FALSE
```

```
Output_url= “$(RAD_DATA_DIR)/spdb/ac_posn”
```

```
output ascii= FALSE;
```

```
EsdAcIngest -params EsdAcIngest.archive -f $RAD_DATA_DIR/telemetry/*.y11
```

```
Cd $RAD_DATA_DIR/spdb/ac_posn
```

```
cd projDir/data/
```

```
scp -r pmvelu@caipeex2011/caipeex2011 -xls
```

```
scp pmvelu@10.2.6.53:CAIPEEX/CAIPEEX-cases.xls /home/titan5
```

```
caipeex-storms-complete01.txt
```

```
Tracks2Ascii -print_params > Tracks2Ascii.caipeex
```

```
Tracks2Ascii -params Tracks2Ascii.caipeex -start "2011 09 21 0 0 0" -end "2011 11  
11 23 59 59" > CAIPEEX-storms-complete01.txt
```

TITAN Command for Statistics

```
cd /home/titan5/projDir/titan/params/
```

Edit ‘Titan.archive’ file and save it with different name (eg. Titan.test), so that the changes are saved.

```
Titan -params Titan.test (for real time)
```

```
Titan -params Titan.test -start “2011 09 21 000” -end “2011 11 09 23 59 59”
```

```
(archive mode)
```

```
Then run: Rview -params Rview.ops
```

Write the data in ascii format

```
Tracks2Ascii -print -params > Tracks2Ascii.caipeex
```

```
Tracks2Ascii -print -params > Tracks2Ascii.caipeex -start "2011 09 21 0 0 0" -end  
"2011 11 11 23 59 59"
```

```
Tracks2Ascii -params Tracks2Ascii.caipeex -start "2011 09 21 0 0 0" -end "2011 11 11 23 59 59"
```

Now check caipeex-storms-complete01.txt in “anal” directory
projDir/ingest/params

Ingesting S-band Radar data

```
SigmatRaw2Dsr-2010.ops FmqMon.ops, Dsr2Vol
SigmetRaw2Dsr -print_params > Dsr2Vol.archive
scp -r pmvelu@10.2.6.53:CAIPEEX/sigmat
mdv/radar/polar_hyd/20111003
Edit sigmetRaw2Dsr.ops (cd home/titan5/projDir/ingest/params) and change as
follows:
debug=*****
instance=*****
input_dir="$(HOME)/projDir/data/sigmat"
output_fmqs_url= "home/titan5projDir/data/fmq/sigmat"
output_fmqs_size=500000000;
output_fmqs_nslots=100000;
SigmetRaw2Dsr -params SigmetRaw2Dsr.archive -f
home/titan5/projDir/data/sigmat/ HYD1111003.RAW*
Fmq -fall message queue
Edit SigmetRaw2Dsr.archive
Radmon -print_params >RadMon.imd
fmqs_url= "fmqs://localhost::/home/titan5/projDir/data_fmqs/sigmat"
Radmon -params RadMon.imd
Fmq -print_params>FmqMon.imd
Fmq -params FmqMon.imd
Input_url= "home/titan5/projDir/data/fmq/sigmat"
Dsr2Vol -print_params > Dsr2Vol.imd
input_fmqs_url= "fmqs://localhost::/home/titan5/projDir/fmq?sigmet"
output_cart_file=TRUE;
cart_file= {400,20,0.5,1,TRUE, "/home/titan5,projDir/data/mdv/radar/cartHyd, -1}
Dsr2Vol -params Dsr2Vol.imd
cd projDir/display/params
```

Edit Rview.ops and save it.

```
#fc dBZ /home/titan5/projDir/data/$(RADAR_CART_DIR) DBZ 720 dbz_color dbz_gray 0.0 100.0 5.0
```

```
#fc dBZ /home/titan5/projDir/data/mdv/radar/cartHyd DBZ 720 dbz_color dbz_gray 0.0 100.0 5.0
```

```
#fc dBZ /home/titan5/projDir/data/mdv/radar/cartHyd VEL 720 vel_color vel_gray 0.0 100.0 5.0
```

```
Home/titan5/projDir/data/eec
```

```
scp -r pmvelu@10.2.6.53:sample-x-band-data
```

Analysis of randomized cases with TITAN:

Once the storm number is identified, the TITAN window of storm history could be used to derive useful information in this regard.

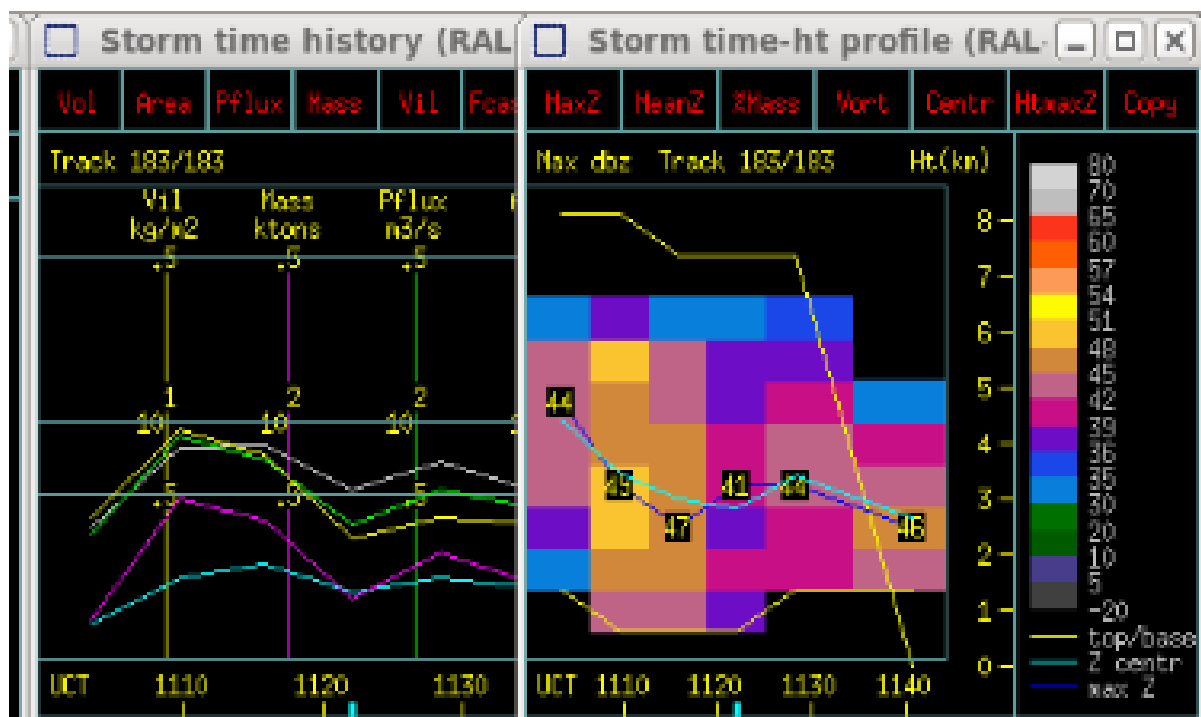


Figure 3.5: TITAN window

Table 3.2 TITAN derived storm parameters for the four randomized seeded cases during 2011 CAIPEEX

Date	28/10/2011	Time	10:41:00	Case #	1					
Time	1041	1047	1053	1059	1106	1112	1118	1124		
Volume	0	98.6	130.2	121.5	104	97.2	48	71		
Area	0	24	31	35	31	31.5	19	25		
Pflux	0	55	75	40	26	23	21.5	20.5		
Mass	0	35.3	53	25.6	17.7	15.4	10	12.5		
Vil	0	4.2	6.3	1.9	1.4	1.6	1.8	1.2		
Date	27/10/2011	Time	11:49:30	Case #	2					
Time	1155	1201	1207	1214	1220	1226	1232	1238	1245	1257
Volume	51.38	57.41	73.7	123	155	169	160	167	158	97
Area	21.74	22.66	25.32	37.35	49.97	58.21	55.85	62.39	67.81	40.59
Pflux	30.75	44	52	72.68	98.62	90.74	64.15	52.1	49.29	29.19
Mass	13.38	21.14	26.4	29.5	51.38	46.63	38.93	30.33	24.63	15.16
Vil	1.71	5.13	5.28	3.78	8.35	5.66	5.21	2.75	2.2	0.98
Date	28/10/2011	Time	8:45:45	Case #	3					
Time	852	858	904	910	916	923	929			
Volume	0	0	75	184	363	473	558			
Area	0	0	21.7	53.5	82.3	88.2	118			
Pflux	0	0	35.3	86	220.5	233	268			
Mass	0	0	19.19	49	134	184	189			
Vil	0	0	2.7	4	10.7	12.8	8.1			
Date	28/10/2011	Time	9:41:41	Case #	4					
Time	947	954	1000	1006	1012	1018				
Volume	74.4	151	146	120	89	44				
Area	20.6	34.6	35.4	32.3	29.5	17.2				
Pflux	59.4	143.5	62.2	31.6	26.4	11.7				
Mass	31.6	85.3	47.5	22	15.3	5.6				
Vil	5.5	10.2	4.1	1.9	1.5	1.1				

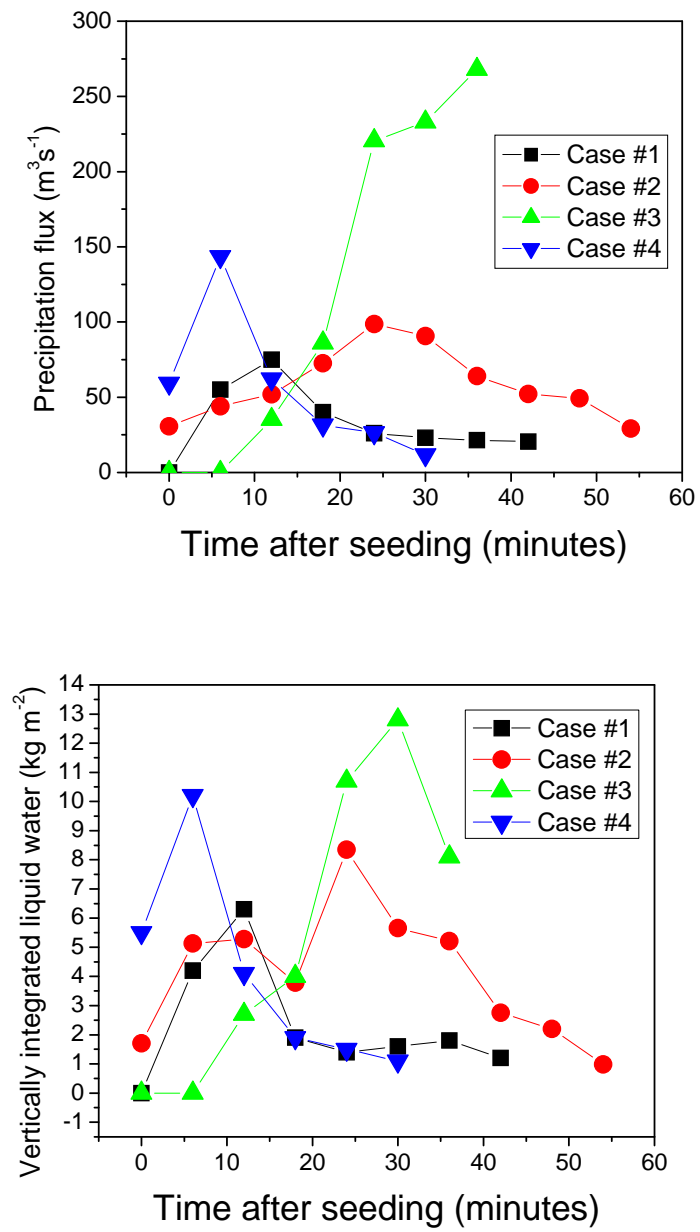


Figure 3.6: A sample of results from Table 3.2, time history of precipitation flux and vertically integrated liquid in the seeded storms after seeding.

Theme 4

Radiation data summary

Contributors:

Padmakumari B., G. Pandithurai, Stuart Piketh, Thara Prabhakaran

Introduction

The research aircraft was instrumented with two Eppley Precision Spectral Pyranometer (PSPs) sun and sky pyranometers sensitive to 0.285 to 2.8 μ m and two Eppley Precision Infrared Radiometers (PIRs) sensitive to 3.5 to 50 μ m. The specifications for the two instrument types are given in (Table 6). One instrument of each type was mounted on the top and the bottom of the aircraft level to the typical angle of flight of the aircraft at research flight speeds. The data from the four instruments are too sensitive to be measured directly on the PADS airborne data acquisition system. The signals from each instrument were recorded on a Campbell Scientific CR10X logger. The signals were resolved on the logger and then transmitted to the PADS system. The installation of the radiation instruments on the Aerocommander 690A (ZS-JRA) is shown in Figure 4.1.



Figure 4.1: Picture of radiation instruments mounted on top and belly of the aircraft

Table 4.1 Specifications of radiometers

Specifications for EPPELY – PSP and EPPELY – PIR broadband radiometers		
EPPELY - PSP Broadband Radiometer		EPPELY - PIR Broadband Radiometer
Sensitivity:	approx. 9 $\mu\text{V}/\text{Wm}^{-2}$	approx. 4 $\mu\text{V}/\text{Wm}^{-2}$
Impedance:	approx. 650 Ohms	approx. 700 Ohms
Temperature Dependence	$\pm 1\%$ over ambient temperature range -20 to +40°C	$\pm 1\%$ over ambient temperature range -20 to +40°C
Linearity:	$\pm 0.5\%$ from 0 to 2800 Wm^{-2}	$\pm 1\%$ from 0 to 700 Wm^{-2}
Response time:	1 second (1/e signal)	2 seconds (1/e signal)
Cosine:	$\pm 1\%$ from normalization 0-70° zenith angle; $\pm 3\%$ 70-80° zenith angle.	better than 5%
Mechanical Vibration:	tested up to 20 g's without damage	tested up to 20 g's without damage

Requirements for installation of the radiation sensors:

The sensors should be grounded to the aircraft ground, which is critical for measuring small signals, otherwise there may be feedback from the aircraft as aircraft generates 900 amps of power.

The instruments used in CAIPEEX-2011 have internal pressure and temperature sensor in the dome. The signal from radiometers are in millivolt and are registered with a Campbell Scientific data logger and an analogue to digital converter, then the signal is fed to PADS software. The temperature and pressure sensors are used to describe the mechanical and thermodynamic influence on the dome, which indeed determines also the accuracy of the measurement. Dome has to be cleaned with deionized water before and after each flight. Special care should be taken that no shadow falls on the radiometers.

Methods

Bucholz et al 2008, JAOT gives a detailed description of the method, and key points relevant to CAIPEEX observations are summarized below. The broadband irradiance or the flux density incident on unit area per unit time is given by,

$$F = \int_0^{\infty} \int_0^{2\pi} \int_0^{\pi/2} I(\theta, \phi, \lambda) \cos\theta \sin\theta \, d\theta \, d\phi \, d\lambda,$$

$I(\theta, \phi, \lambda)$ is the radiance at a given wavelength λ incident on unit area from a given zenith θ and azimuth ϕ angle. Note that integration is carried out over complete angle. This general definition gives the irradiance with respect to the given unit area regardless of the orientation

of that unit area. The amount of radiative energy deposited at a given altitude of the atmosphere that is of specific interest and this is given by the irradiance, F_E , for a unit area that is horizontally level with respect to earth-centered coordinates (see in the Figure 4.2a). The goal of aircraft-mounted radiometers is to measure F_E , but what they actually measure is F_R , the irradiance with respect to the unit area that is horizontally level with respect to the radiometer (see Figure 4.2b)

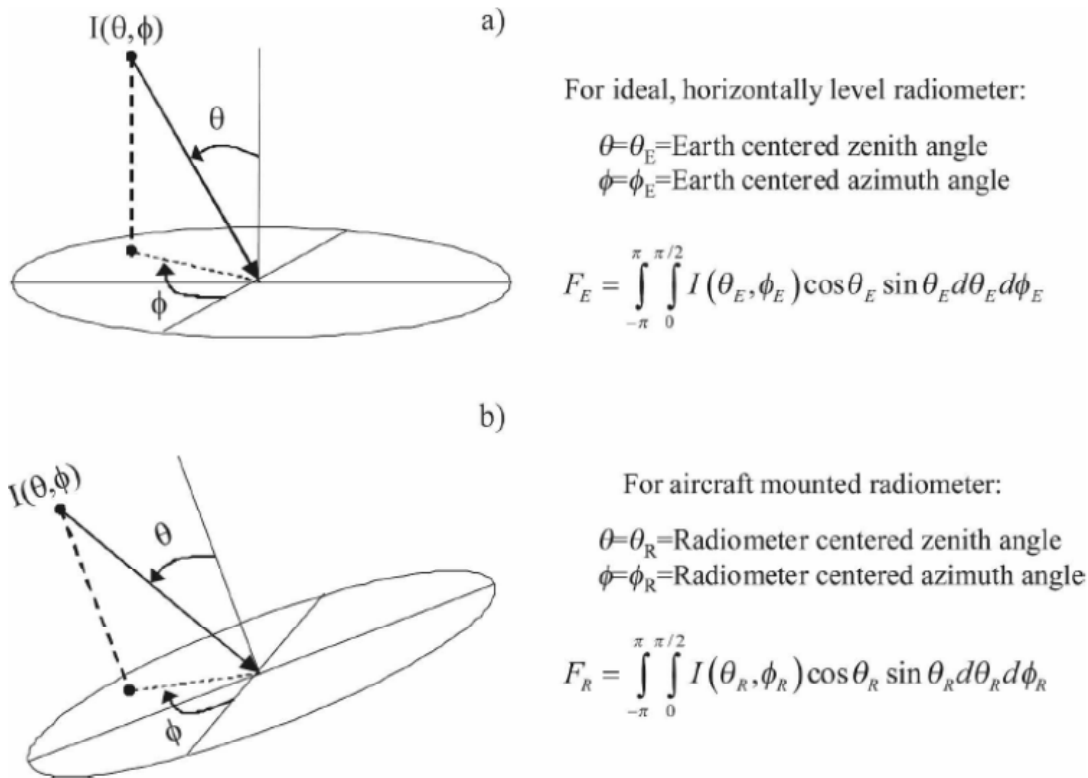


Figure 4.2: Irradiance, F_E , for a unit area that is horizontally level with respect to earth-centered coordinates (a) and the irradiance with respect to the unit area that is horizontally level with respect to the radiometer (b) (source: Bucholz et al 2008, JAOT)

The aircraft will seldom fly at horizontal level and the radiometer will never be at horizontal level with respect to earth centered coordinates and the measured irradiance F_R differs from F_E . The magnitude of this difference will vary depending on the degree of tilt of the radiometer and the angular distribution of the incoming radiation across the sky. The difference is minimal for a nearly level radiometer measuring a nearly isotropic radiation field, but the difference increases as the tilt of the radiometer becomes greater and the radiation field becomes less isotropic.

The downwelling sunlight at a given altitude can be thought of as consisting of two components: the radiation coming directly from the sun, $I_{\text{solar,dir}}$, and the diffuse sunlight, $I_{\text{solar,diff}}$, scattered from the complete hemisphere by the air (i.e., Rayleigh scattering) and particles in the atmosphere (clouds, dust, pollution, etc.). The aircraft-measured downwelling solar irradiance with respect to radiometer centered coordinates, $F_{\text{solar},R}$, can therefore be expressed into two terms, a direct and diffuse component:

$$F_{\text{solar},R} = \pi I_{\text{solar,dir}}(\theta_{R0}, \phi_{R0}) \cos\theta_{R0} + \int_0^{2\pi} \int_0^{\pi/2} I_{\text{solar,diff}}(\theta_R, \phi_R) \cos\theta_R \sin\theta_R d\theta_R d\phi_R.$$

Changes in solar zenith angle with respect to the radiometer will change the measured irradiance, even though the sun's positions in the sky and the direct component of the intensity, $I_{\text{solar,dir}}$, have not changed. Since the direct solar radiation is usually the more dominant term it is typical to see significant changes in the measured solar irradiance generated by nothing more than heading changes in the aircraft.

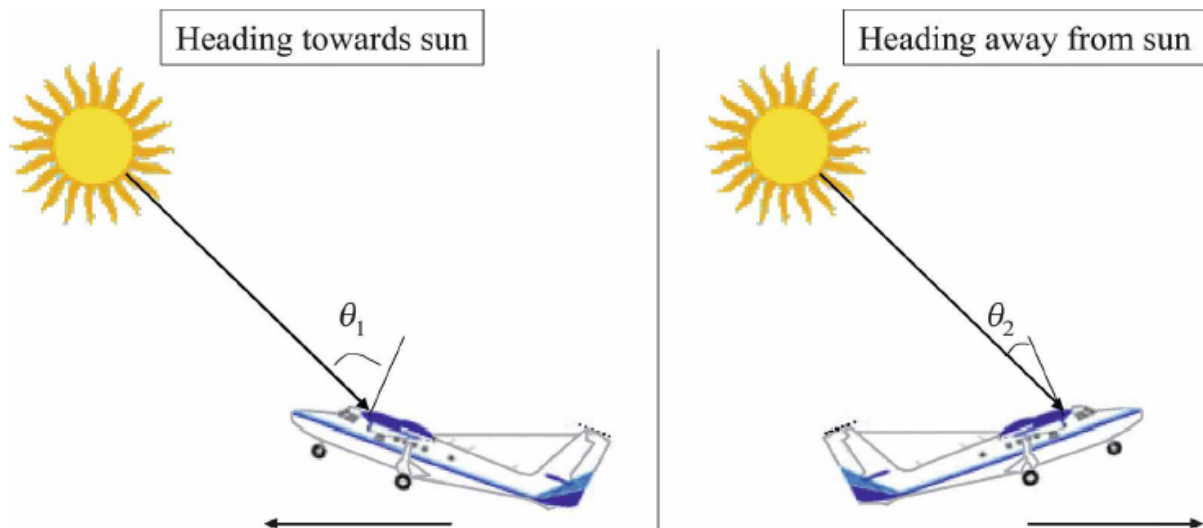


Figure 4.3: Effect of solar zenith angle, aircraft pitch, and aircraft heading on the zenith angle of the sun with respect to the aircraft normal. In both pictures the solar zenith angle with respect to earth-centered coordinates is approximately 45° , and the aircraft is pitched up at 20° (an exaggerated pitch angle for illustrative purposes). However, the solar zenith angle with respect to the aircraft normal is greater when (left) heading toward the sun than when (right) heading away from the sun, even though the true solar zenith angle has not changed. Since irradiance sensors have a cosine angular response, radiometers rigidly mounted on a pitched-up aircraft will measure a direct solar irradiance that is less when heading into the sun than when heading away from the sun. (source: Bucholz et al 2008, JAOT)

To obtain an altitude profile of the irradiance a “stacked” flight pattern is typically flown where the aircraft sequentially flies straight and level legs at multiple altitudes over the same geographic line. The drawbacks to this type of flight profile are that the data are obtained at only a limited number of discrete altitude levels and it can take a long time to complete. Any given leg can be from a few minutes to tens of minutes long, and when the time for climbing, descending, and maneuvering are added in a complete altitude stack can take an hour or more to complete. During this time the atmospheric conditions can change significantly making it difficult to relate the data from the top and bottom of the stack. The vertically stacked flight track may look like in Figure 4.4.

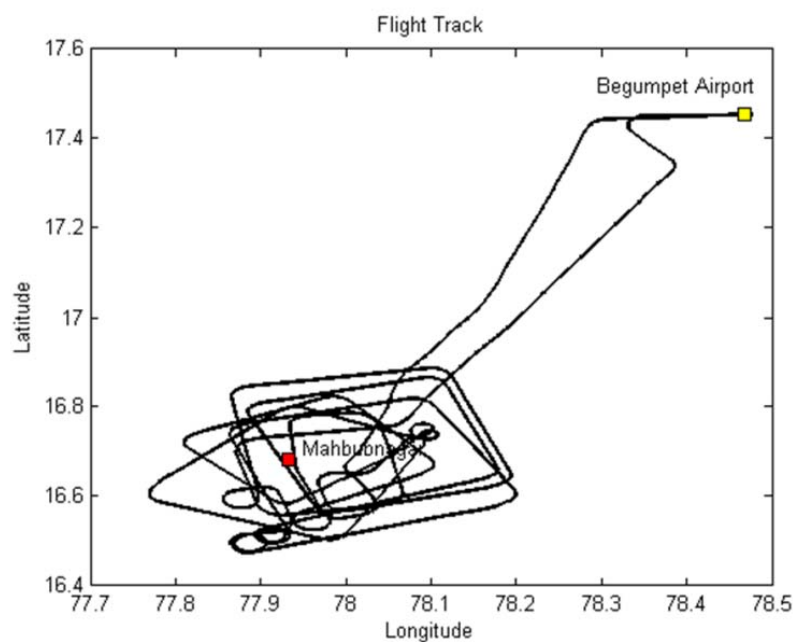


Figure 4.4: Box patterned flight track corresponding to a radiation flight

Usually any measurements made for pitch and roll angles greater than $\pm 2^\circ$ to $\pm 5^\circ$ are not analyzed. Depending on the flight patterns this procedure can eliminate a large fraction of the radiometer data from any given flight. This will eliminate data at the corners of the boxes.

Further corrections required for this data are

- 1) Coordinate transformations that use the airplanes navigational information (time, latitude, longitude, altitude, pitch, roll, and heading) and solar ephemeris data to determine the zenith and azimuth angles of the sun with respect to the rigidly mounted radiometer in order to scale the direct component of the measured solar irradiance back to earth-centered coordinates (Hammer et al. 1991)

2) Iterative methods where the total measured irradiance (direct plus diffuse) is scaled by a range of offsets to the aircraft's pitch and roll values until the optimum pitch and roll offset pair is found, which minimizes the differences between downwelling irradiances at heading changes (Bannehr and Glover 1991; Saunders et al. 1992; Bannehr and Schwiesow 1993; Valero et al. 1997; Boers et al. 1998).

The correction methods assume that the pitch and roll of the aircraft match the pitch and roll of the sensor. However, if the mounted sensor is not level with respect to the latitudinal and longitudinal axes of the aircraft then there may be unknown offsets between the pitch and roll of the aircraft and the pitch and roll of the sensor that limit the effectiveness of these correction methods.

The steps for radiation corrections:

1. Zenith angle corrections
2. Pitch and roll corrections

Status of data and availability

Calibrated data is available in netCDF and ascii formats along with other CAIPEEX datasets. The measurements taken for solar and terrestrial radiation require a lot of post-collection scrutiny to determine if there were any external factors interfering with the recorded signal. These factors might include cloud cover and aircraft pitch, yaw, and roll angles. These corrections are not applied to the data set. The detailed analysis and corrections are needed at a case by case analysis and care should be practiced in using the data.

A case study

One case study of the vertical profile of the radiation measurements in relation to the other measured variables is presented to give a sense of the data collected. The data was used only if the aircraft was flying straight and level (pitch, roll, and yaw angles smaller than 5 degrees). An example is taken from a flight conducted to the south east of Hyderabad on 27 October 2010 between 10:46:56 and 11:02:18 UTC. The vertical profiles for aerosols, trace gases, and radiation measurements are given in Figure 4.5. Every vertical profile conducted for the entire flight campaign has been extracted and analyzed as shown in Figure 4.5. The extensive case study on 27 October shows good vertical structure in all the parameters. Trace gas and aerosols concentrations seem to follow each other fairly closely

and are a function of the vertical thermodynamic structure of the atmosphere. It is also clear that the radiation measurements are affected by the vertical structure observed in the other parameters. These relationships will be complex and will require significantly more analysis to resolve in any meaningful scientific outcome.

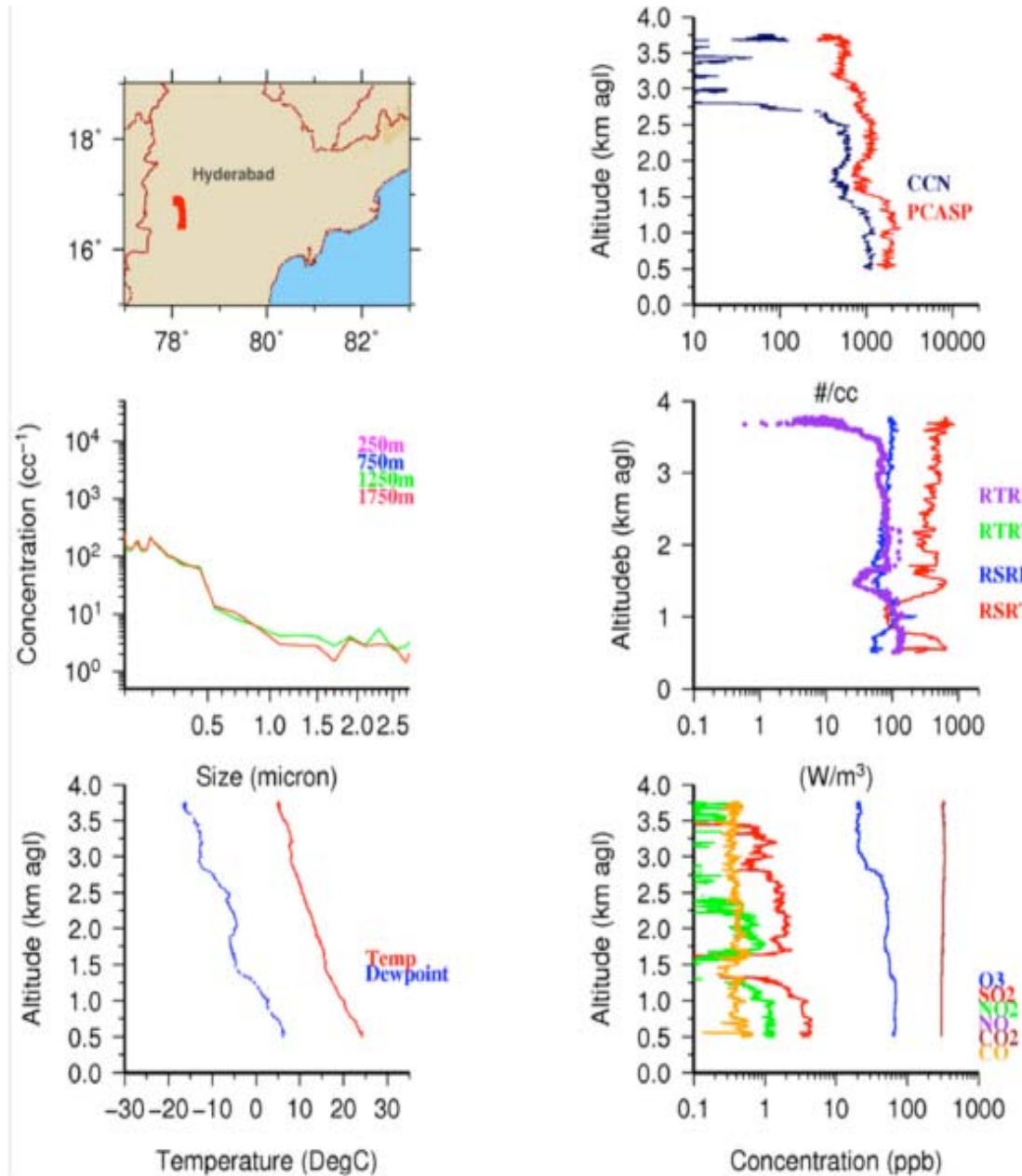


Figure 4.5: An example of a vertical profile conducted south east of Hyderabad on 27 October 2010 between 10:46:56 and 11:02:18 UTC; Top Left: flight path; Top Right: profile of fine mode aerosols and CCN concentrations; Middle Left: size distribution of fine mode aerosols at different altitudes; Middle Right: radiation measurements RTRB – terrestrial radiation bottom of aircraft, RTRT – terrestrial radiation top of aircraft, RSRB – solar radiation bottom of aircraft, RSRT – solar radiation top of aircraft; Bottom Left: vertical temperature and dew point profile; Bottom Right: vertical profile of trace gas measurements (discussed in the next theme)

Theme 5

Trace gas data summary



Contributors:

R S Maheskumar, Yogesh Tiwari, Stuart Piketh, T. Prabhakaran

Introduction

The instruments used in 2010 experiment for trace gas data are from Thermo for SO₂, O₃, NO and NO₂, CO. The samplers are shown in Figure 5.1. These are typically used for ground observations. These sensors are not the ones with best sensitivity, but they are more robust with performance in extreme conditions, are less sensitive to temperature variations. NOx sensor has a very sophisticated cooling system.

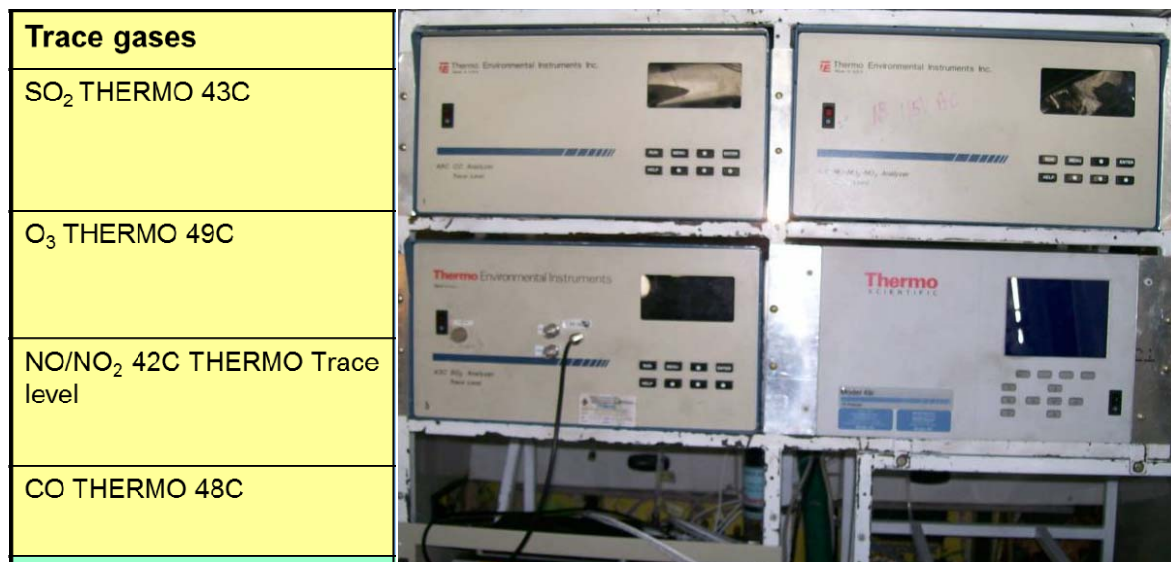


Figure 5.1: Trace gas instruments

Trace Gases instruments and their range

- ❖ TECO SO₂ (43c) Sulfur dioxide 0 to 1000 ppb
- ❖ TECO O₃ (49i) Ozone 0 to 1000 ppb
- ❖ TECO NO_y (42c) Nitrogen oxides 0 to 1000 ppb
- ❖ TECO CO (48c) Carbon monoxide 0 to 10,000 ppb
- ❖ LICOR 7000 series Carbon Dioxide 0 to 500 ppm

Inlet:

Sample air is drawn into the aircraft through an inlet and then distributed to the various instruments. The sample line for the trace gas instruments is regulated with mass flow controller through a joint manifold (Figure 5.2). The mass flow controller is set to cater for sufficient air flow to each instrument at ground level (typically around 4 l.min⁻¹). The full pumping capacity of the system is 10 l.min⁻¹. As the aircraft climbs with altitude the flow is kept at a constant 4 l.min⁻¹. This ensures that the instruments always have sufficient flow. Above 14 000 ft or 4500 m the instruments will start to experience low flow alarms. All data above this altitude should be viewed as unreliable.

The inlet system used on the aircraft consists of a stainless steel nozzle mounted approximately 30 cm from the fuselage, half a meter aft from the aircraft windscreen. The nozzle is based on a NACA 1 series inlet, with an inlet diameter of 15.4 mm, and a maximum

radius of 48 mm. The nozzle lip is reduced to a 3-mm radius. A 5-degree diffuser cone brings the internal diameter to 34 mm, where the nozzle joins onto the inlet pipe. The pipe has two bends in it to bring it inside the aircraft cabin, where it runs parallel to the cabin roof. There are several points along the pipe for connection of instrumentation. The stainless steel pipe is then connected to a flexible hose, and the exhaust is routed through the pressure bulkhead at the rear of the cabin. The inlet system exhaust is underneath the fuselage, a simple unfaired pipe with a 45 degree rake. Typical true airspeeds are between approximately 70 and 130 m/s, corresponding to indicated airspeeds of 130 kts to 180 kts at up to 21,000-ft altitude.

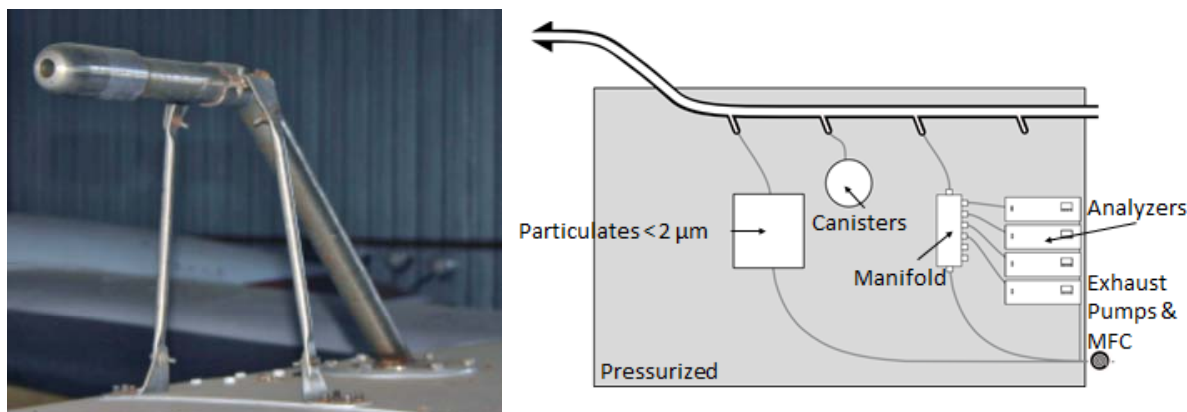


Figure 5.2: Inlets

Principles of operation of various trace gas samplers are given below:

Sulfur Dioxide

Model 43C SO₂ analyzer is based on the following characteristics of SO₂ molecules. SO₂ molecules get excited as they absorb ultraviolet (UV) light at one wavelength. While decaying to a lower energy state, they emit light at a different wavelength. The air sample is taken through the inlet and hydrocarbons are removed. In the fluorescence chamber a pulsating UV light is reflected off four selective mirrors that only reflect light at the specific wavelength to excite SO₂ molecules. The UV light emitted by the SO₂ molecules decaying to a lower energy level is proportional to the SO₂ concentration. The photo multiplier tube (PMT) only receives the UV light emitted by the decaying SO₂ particles.

Ozone

Ozone molecules absorb UV light at a wavelength of 254 nm and the degree of UV absorption is directly related to the ozone concentration, following the Beer-Lambert Law. The air sample is drawn into the analyzer through the SAMPLE bulkhead, where it then splits into two gas streams. The one gas flows through an ozone scrubber and is known as the reference gas, which flows to the reference solenoid valve. The second gas is known as the sample gas and flows directly to the sample solenoid valve. The reference and sample gas streams are alternated between cells A and B every 10 seconds, where the UV light intensities of each cell are measured by detectors in the cells.

The switching of gas streams between the cells allows the cells to be flushed, and the light intensities are ignored during this period. The average calculated ozone concentration for each cell is sent to the front panel display and the analogue outputs.

Nitric Oxide:

The operation of the Model 42C is based on the principle that the nitric oxide (NO) concentration is linearly proportional to the luminescence that is produced with the reaction between NO and O₃. Infrared light is emitted when electronically excited NO₂ molecules decay to a lower energy state

Before nitrogen dioxide (NO₂) can be measured using the chemiluminescent reaction, it must be transformed into NO. This conversion occurs by molybdenum NO₂ to NO converter heated to about 325°C. The air sample is drawn in through the SAMPLE bulkhead and flows through the particulate filter, a capillary and to the mode solenoid valve. The sample is routed through the NO₂ to NO converter and to the reaction chamber in NO_x mode, or straight to the reaction chamber in NO mode. Dry air enters through the DRY AIR bulkhead and then flows through a flow sensor and through a silent discharge ozonator (ozone needed for the chemiluminescence reaction is generated here). Electronically excited NO₂ molecules are produced when the NO in the air sample reacts with the ozone. NO₂ luminescence is detected by a PMT. The concentration of NO and NO_x calculated in NO and NO_x mode are stored in memory, and the difference between the concentrations is used to calculate the NO₂ concentration. The analyzer outputs NO, NO₂, and NO_x concentrations to the front panel display and to the analog outputs.

Carbon monoxide

The principle of CO analysis is based on the characteristic feature of CO to absorb infrared radiation at a wavelength of 4.6 μm. Instrument electronics of the Model 48C need to convert the basic analyzer signal to a linear output, as infrared absorption has a non-linear relationship. An exact calibration curve is used to linearize the instrument output over any range up to a concentration of 10,000 parts per million (ppm). The sample is drawn in through the SAMPLE bulkhead and flows through the optical bench. An infrared source emits radiation that is passed through alternating CO and N₂ filters. Absorption of the sample gas occurs in the optical bench once the radiation has passed through a narrow band pass interference filter and the infrared radiation exits the optical bench and falls on the infrared detector. The CO gas filter produces a reference beam, which cannot be further attenuated by CO in the sample cell. A measurement beam that can be absorbed by CO in the cell is produced in the N₂ side of the filter wheel, which is transparent to infrared radiation. Modulation of the chopped detector signal occurs through alternating filters that have amplitude related to the concentration of CO in the sample cell. This system responds specifically to CO, as other gases absorb the reference and measure beams equally and do not cause modulation of the detector signal. The outputs of the CO concentration are visible on the front panel display and the analogue output.

Carbon dioxide

The instrument used to measure CO₂ (Figure. 5.3) on the aircraft was a Licor 7000 (LI-7000). The LI-7000 is a differential, non-dispersive, infrared (NDIR) gas analyzer. The CO₂ and H₂O measurements are based on the difference in absorption of infrared (IR) radiation passing through two gas sampling cells. Cell A (normally the reference cell) is used for a gas of known CO₂ or H₂O concentration, and Cell B (normally the sample cell) is used for a gas of unknown concentration. Infrared radiation is transmitted through both cell paths, and the radiation at the detectors is measured in both cells and used to compute absorption (extracted out of LI-7000, CO₂/H₂O Analyzer - Instruction Manual).

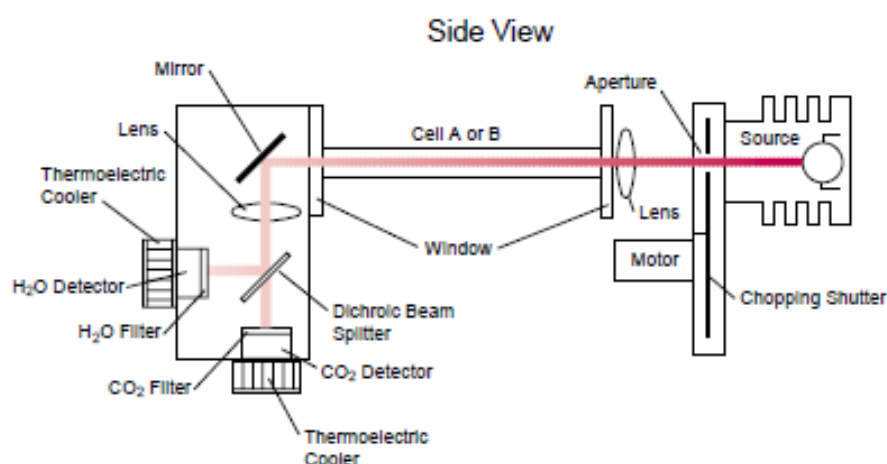


Figure 5.3: Schematic of LI-7000 optical path

All trace gas instruments should be calibrated to obtain representative results from any aircraft or ground based campaign. In order to perform a full dynamic calibration it is essential to have a trace gas calibrator. A full dynamic calibration (one that test the linearity across the entire measuring range of the instrument) should at the very least be conducted before the start of the campaign and again at the end of the campaign. This is to test the linearity of the analyzer.

In addition zero and span checks should be conducted throughout the campaign to ensure that there is no detectable drift on the analyzer measurements.

Zero check is to be carried out for SO₂, NO_x, O₃, which is carried out with Purafil or activated carbon on the inlets, which strips out the trace gases and leaves a zero signal. For CO₂ sodium carbonate is used. For CO SAFNOCAT is used. In flights where we need to have accurate measurements at different vertical levels, the zero check is to be carried out at each level. Sometimes 1-5 min circles are required and to remove the background value. This is for baseline check at each altitude.

Span check is done with a calibration gas, zero air and a calibrator. The calibrator is basically a pair of mass flow controllers which are used to mix the span gas and the zero air in known ratios. The gases are typically mixed in a Teflon mixing chamber and that makes the calibration sample.

Reliable source of calibration gases is essential for accurate measurements. The

Corrections for Data

$$X_{corrected} = X_{uncorrected} \times \frac{[T_c \times P]}{[T \times P_c]}$$

X: Gas concentration
Tc: Calibration temperature
Pc: Calibration pressure
T: Actual temperature
P: Actual pressure

Important points regarding Potential errors with data:

1. Instrument response time - 0-span (30 sec on ground – increased error due to speed of aircraft – shorter exposure to peak - underestimate plume concentrations
2. Instrument inconsistent sensitivity to pressure change – especially CO₂
3. Instrument flow – high altitude low flow – despite the back constant flow system – best data under 14000 ft

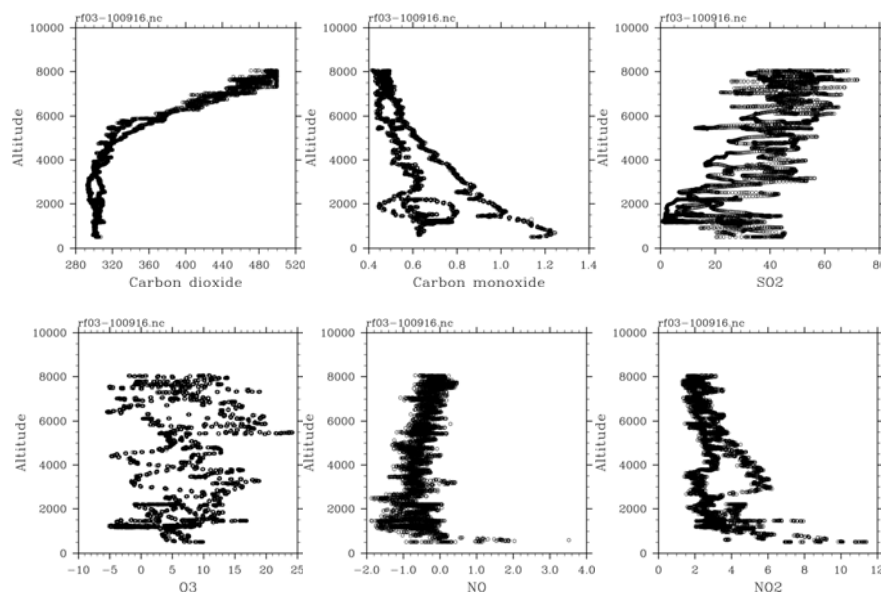


Figure 5.4 An example of trace gas data from a research flight during 2010. Note that CO₂ observations beyond 4 km are erroneous due to the points discussed above. It may also be noted that CO₂ observations showed lower concentrations, which is being investigated. The recovery time is to be checked for this. Few of the analyzers also showed negative concentrations, which are also erroneous values. It is to be investigated from the flight report whether the analyzers were functioning on the aircraft on a case by case basis before making any conclusions/assumptions.

References

- Bannehr, L. and Glover, V., 1991: Preprocessing of airborne pyranometer data. NCAR Tech. Note NCAR/TN-364+ STR, 35pp.
- Bannehr, L. and Schwiesow, R., 1993: A technique to account for the misalignment of pyranometers installed on aircraft, *J. Atmos.Oceanic Technol.*, 10, 774 –777.
- Boers, R., Mitchell, R.M. and Krummel, P.B., 1998: Correction of aircraft pyranometer measurements for diffuse radiance and alignment errors. *J. Geophys. Res.*, 103, 16753 – 16758.
- Bucholtz et al, 2008: The Stabilized Radiometer Platform (STRAP) - An Actively Stabilized Horizontally Level Platform for Improved Aircraft Irradiance Measurements, *JTECH*, 2161-2175, DOI:10.1175/2008JTECHA1085.1
- Hammer, P.D., Valero, F.P.J. and Kinne, S., 1991: The 27–28 October 1986 FIRE cirrus case study: Retrieval of cloud particle sizes and optical depths from comparative analyses of aircraft and satellite-based infrared measurements, *Mon.Wea. Rev.*, 119, 1673–1692.
- Saunders, R.W., Brogniez, G., Buriez, J.C., Meerkotter, R. and Wendling, P., 1992: A comparison of measured and modelled broadband fluxes from aircraft data during the ICE '89 field experiment, *J. Atmos. Oceanic Technol.*, **9**, 391–406.
- Valero, F.P.J. and Coauthors, 1997: Atmospheric Radiation Measurements Enhanced Shortwave Experiment (ARESE): Experimental and data details, *J. Geophys. Res.*, 102, 29929 – 29937.